Internal structure of the Martian south polar layered deposits

S. Byrne
Massachusetts Institute of Technology, Cambridge, Massachusetts, USA

A. B. Ivanov
Jet Propulsion Laboratory, Pasadena, California, USA

Received 20 March 2004; revised 8 August 2004; accepted 20 August 2004; published 9 November 2004.

[1] We investigate the three-dimensional (3-D) stratigraphic structure of the south polar layered deposits (SPLD) on Mars. Prominent bench-forming layers exposed on SPLD scarps were observed and mapped in three dimensions using high-resolution topographic and imaging data sets. Using the 3-D location of exposures of one of these strata, we can accurately describe the shape of that layer using simple mathematical functions. Analysis of these functions and the surface topography can be used to reliably predict where on other scarps this layer is exposed. In general this bench-forming layer (and its surrounding strata) is not flat and is well approximated as a parabolic dome near the center of the SPLD. Its curvature indicates that when deposited it was draped over a topographic dome similar in size to that of the present day. The scarps in which this layer is exposed must have formed subsequently and have not been significantly modified by flow processes. The basement topography exercises some control over the shape of the interior strata in extreme cases. Our successful layer-fitting technique illustrates the regional uniformity in layer formation and the lack of major internal defects (such as faulting) within the SPLD. We have mapped exposures of what appear to be this layer in scarps farther from the center of the deposits. The position of these exposures can be used to modify the modeled parabolic shape at the periphery of the SPLD. These peripheral elevations provide constraints on the role of flow in the overall shaping of the SPLD. *INDEX TERMS:* 5462 Planetology: Solid Surface Planets: Polar regions; 5416 Planetology: Solid Surface Planets: Glaciation; 5415 Planetology: Solid Surface Planets: Erosion and weathering; 5464 Planetology: Solid Surface Planets: Remote sensing; 6225 Planetology: Solar System Objects: Mars; *KEYWORDS:* ice, Mars, stratigraphy

Citation: Byrne, S., and A. B. Ivanov (2004), Internal structure of the Martian south polar layered deposits, *J. Geophys. Res.*, *109*, E11001, doi:10.1029/2004JE002267.

1. Introduction

[2] The topographic dome of Planum Australe, which is composed of the south polar layered deposits (SPLD) and partially covered by the southern residual CO_2 cap, was first observed by spacecraft during the Mariner 7 flyby several decades ago [*Sharp et al.*, 1972]. Exposures of its layered interior can be seen in the many troughs and scarps which incise it, and were first observed in Mariner 9 images [*Murray et al.*, 1972]. At the time of discovery these deposits were immediately recognized as a possible record of Martian climate [*Cutts*, 1973b; *Ward*, 1973; *Cutts and Lewis*, 1982]. These polar layered deposits are commonly interpreted as being composed of varying proportions of atmospherically deposited water ice and dust [*Clifford et al.*, 2000; *Thomas et al.*, 1992; *Cutts*, 1973b]. Modeling of the shape and thermal properties of the SPLD has shown that CO_2 ice is not an important constituent [*Nye et al.*, 2000; *Mellon*, 1996]. The topographic dome of the SPLD is roughly parabolic and at its maximum height stands 3 km above the surrounding southern highlands [*Smith et al.*, 2001]. Its highest point is offset ~3° from the rotational pole at 87.3°S, 349°E. In the longitude range −90°E to 90°E the SPLD have a stair-step structure with distinct scarps separated by relatively flat areas, as shown by the topographic cross section in Figure 1. On the other side of the rotational pole (longitude range 90°E–270°E) the SLPD extend equatorward as a broad flat plateau [*Tanaka and Scott*, 1987]. The SPLD are bounded by a steep scarp over longitudes −90°E–160°E, whereas from 160°E–270°E they gradually thin into the underlying terrain.

[3] The surface of the SPLD is mantled with a cohesive but low thermal inertia material which is likely to be a sublimation lag deposit [*Hofstadter and Murray*, 1990; *Vasavada et al.*, 2000; *Herkenhoff and Murray*, 1990b; *Herkenhoff and Vasavada*, 1999; *Paige and Keegan*, 1994]. The thickness of this mantle is unknown and may vary considerably throughout the region. However, locations where it is only millimeters thick and the thermal signature of

0148-0227/04/2004JE002267$09.00

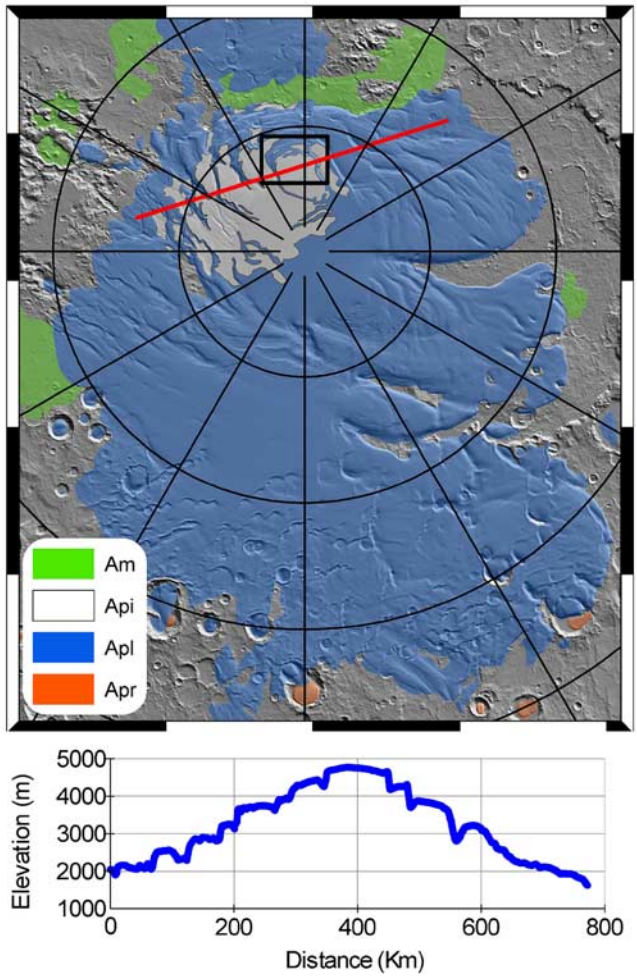

Figure 1. Geologic context of the region studied in this paper. South polar stereographic projection of shaded MOLA topography with parallels and meridians plotted every 5° and 30°, respectively. Geologic units indicated have been mapped and provided by *Kolb and Tanaka* [2001]; Apl indicates the polar layered deposits, and Api indicates the thin covering of CO_2 ice (see text for discussion). Black box includes the highest portion of the layered deposits and indicates the study area shown in Figure 3. Red line indicates the position of the topographic cross section shown in bottom panel. The stair-step character of the layered deposits in this region is apparent.

the underlying water ice shows through, have recently been discovered [*Titus et al.*, 2003]. Draped over the flat areas on the highest portion of the layered deposits is the high-albedo residual ice cap, which is composed of CO_2 ice [*Kieffer*, 1979]. Modeling of morphology within the residual ice [*Byrne and Ingersoll*, 2003] and analysis of neutron returns [*Tokar et al.*, 2003; *Prettyman et al.*, 2004] indicate that the residual CO_2 deposit is only a few meters thick. The cohesive mantle and the residual CO_2 ice are topographically inconsequential in thickness compared with the SPLD.

[4] The scarps which incise the SPLD and which expose its layered interior have been studied by previous investigators. The scarps are centered on the topographic highpoint rather than the geographic pole, as noted by *Weijermars* [1986]. They appear superposed on a quasi-spiral pattern of subdued troughs to the east of the topographic highpoint [*Tanaka and Scott*, 1987]. Various formation mechanisms for these polar scarps have been suggested. *Cutts* [1973a] proposed eolian erosion; however Coriolis deflection would not result in wind blowing along these features. Flow of the layered deposits has been suggested [*Weijermars*, 1986] to explain the curved troughs; however, the flow velocities necessary (0.2 ms^{-1}) to produce a spiral pattern seem prohibitively high. *Howard* [1978] suggested preferential sublimation from inclined surfaces could cause a feedback which encourages their growth into scarps. In this model, material ablated from scarps could be redeposited on the flat interscarp surfaces. This scenario would lead to poleward migrating scarps. In the case of the trough system in the north polar layered deposits, *Fisher* [1993] obtained spiral forms by combining this model with an asymmetric ice flow field. *Hvidberg* [2003] derived the mass-balance profile necessary to counteract poleward trough migration with equatorward ice flow. *Pelletier* [2004] argued that spiral forms can self-organize through preferential ablation and lateral heat conduction, although the timescales required may be prohibitively long. *Ng and Zuber* [2003] considered physical mechanisms behind a spatial instability which leads to trough formation.

[5] Detailed studies of the SPLD (reviewed by *Clifford et al.* [2000]) have considered surface geology [*Tanaka and Scott*, 1987; *Kolb and Tanaka*, 2001; *Herkenhoff*, 2001; *Fishbaugh and Head*, 2001], faulting and mass-wasting at the margins of the deposits [*Herkenhoff et al.*, 2003; *Murray et al.*, 2001], color [*Herkenhoff and Murray*, 1990a], and thermal inertia [*Herkenhoff and Vasavada*, 1999; *Paige and Keegan*, 1994]. Previous studies relate mainly to what is exposed at the surface. This paper seeks to understand the internal structure of the SPLD. First-order questions concerning this structure remain currently unanswered:

[6] 1. Was the deposition regional in scale or local? Accumulation from atmospheric deposition is expected to be uniform over regional scales. However, the mechanics of layer formation are poorly understood; local microclimatological and topographic effects may also influence deposition rates. Investigating the length scales over which stratigraphy is continuous can help establish the importance of local perturbations.

[7] 2. Are the current SPLD a remnant of a formerly larger deposit or is their current extent representative of their historical size? The layering visible in the scarps at the edge of the SPLD indicates that they were originally larger and subsequently eroded back [*Tanaka and Scott*, 1987]. Figure 2 describes two end-member scenarios. If the SPLD were much more extensive in the past and then eroded back to their current size (Figure 2, B–B′) then the strata would be expected to be relatively flat, with a curvature significantly less than that of the surface topography. If on the other hand the internal layering is convex, like the present surface topography (Figure 2, A–A′), then that would indicate that the SPLD were close to their current size when those strata were deposited.

[8] 3. How much does the basement topography affect the shape of the interior strata? The basement topography of

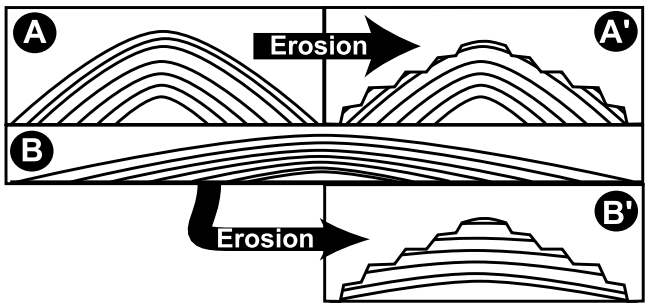

Figure 2. Two end-member situations for the historical extent of the SPLD. Situation A relates to an original topographic structure similar in size to that of the present. Situation B refers to a formerly more extensive deposit. In both cases, erosion reduces the SPLD to their current shape and extent shown in A′ and B′. The degree of curvature of the internal layering can be used to distinguish between these two cases. Panels are shown at the same scale, except B, which has been reduced by a factor of two. The vertical exaggeration is approximately 60.

the SPLD is almost entirely unconstrained. The SPLD have been deposited on the heavily cratered southern highlands [*Tanaka and Scott*, 1987]. These deposits also partially cover the large (~850 Km) Prometheus impact basin [*Wilhelms*, 1973]. The underlying topography could therefore be expected to have considerable relief. It is also possible that the current SPLD cover some remnant polar deposits from a previous epoch, such as those discussed by *Head and Pratt* [2001].

[9] 4. Has the interior of the SPLD been deformed by local/regional processes such as faulting/flow? The degree to which the present layered deposits behave like terrestrial ice sheets is unknown [*Clifford et al.*, 2000]. The possibility of flow has been discussed mostly for the northern polar layered deposits [*Budd et al.*, 1986; *Fisher*, 1993, 2000; *Fisher et al.*, 2002; *Greve*, 2000; *Greve et al.*, 2003; *Nye*, 2000; *Weijermars*, 1986; *Hvidberg*, 2003] but also for the SPLD [*Head*, 2001; *Weijermars*, 1986; *Nye*, 2000]. In terrestrial ice sheets the internal structure of the layers can be used to diagnose flow patterns [e.g., *Ng and Conway*, 2004].

[10] The importance of the polar layered deposits lies in the climatic record that they possibly contain. While the above questions do not relate directly to climate, they are important considerations in how this climatic record should be read. For example, if the internal layering is similar to that depicted in Figure 2 (A′), then layer sequences exposed on upper scarps may be expected to repeat on lower scarps. In this case fewer layers would be available for observation than in the situation depicted in Figure 2 (B′), where each scarp exposes a different sequence. Thus the length of the observable record is governed by the internal shape of these layers.

[11] The original model of internal structure proposed by *Murray et al.* [1972] envisioned the interior of the polar layered deposits to be composed of a stack of flat depositional surfaces or "plates." The lack of relevant data before the Mars Global Surveyor (MGS) mission meant that this view has remained largely uncontested. However, with the advent of high-resolution topographic measurements [*Smith et al.*, 2001] and visible imaging [*Malin and Edgett*, 2001; *Christensen et al.*, 2003] it is now possible to correlate layers over large distances and investigate the structure of the SPLD in three dimensions.

[12] In the course of this work we have identified and investigated several prominent bench-forming layers exposed on SPLD scarps. We report here the results for one such layer. Bench-forming layers in this region were previously observed by *Herkenhoff and Murray* [1990b] using topography derived from Mariner 9 stereophotogrammetry and photoclinometry. They retrieved three elevation and slope profiles which agree well with observations from the Mars Orbiter Laser Altimeter (MOLA). Many of these bench-forming layers appear prominently in the high-resolution gridded MOLA topography available for the south polar region [*Neumann et al.*, 2001]. As one would expect, they also appear within the visible imaging data sets of the same region.

[13] Bench-forming layers typically influence the topography of a scarp due to a higher resistance to erosion than the overlying strata. In the case of these polar layers this resistance could be due to a higher sediment concentration, which limits the rate of escape of water vapor in a sublimation dominated environment. The overlying, less-resistant layers retreat faster, leaving a flat bench part way down the scarp. When compared to surrounding strata, bench-forming layers appear wider in plan-view because of their lower slope, although they may not actually be thicker. Layers below a bench-forming stratum are somewhat protected by it. As these lower layers retreat they undercut the resistant layer. Mass wasting processes can then act so that the bench remains limited in width. The top of each layer in a sedimentary deposit represents a paleosurface of that deposit (isochrone). The top of a bench-forming layer is well approximated by the top of the bench it generates. Topographic benches on scarps within the SPLD are shown in Figure 3. Their morphology (see Figure 4), detailed in section 2.2, is consistent with this general geological description.

[14] In the next section we describe our study area, data sources, and methods used to map these features. We also describe the characteristic morphology and stratigraphic setting of one bench-forming layer, on which we focus for the remainder of the paper. In section 3 we report on how its three-dimensional shape can be accurately described by simple mathematical functions. In section 4 we describe how these functions can be used to predict the location of exposures of this bench-forming layer on scarps outside our initial study area. On the basis of characteristic morphologies and stratigraphic setting, we have also identified exposures of what we interpret to be this bench-forming layer in scarps farther from the deposit center. These more distant exposures are not predicted by the approach described in section 4. Their elevations have important implications for the internal structure of the SPLD. They are discussed in section 5. Results are discussed in section 6 and summarized in section 7.

[15] Latitudes and longitudes quoted in this paper are referenced to the IAU 2000 [*Seidelmann et al.*, 2002] radii and prime meridian. Longitudes increase to the east and

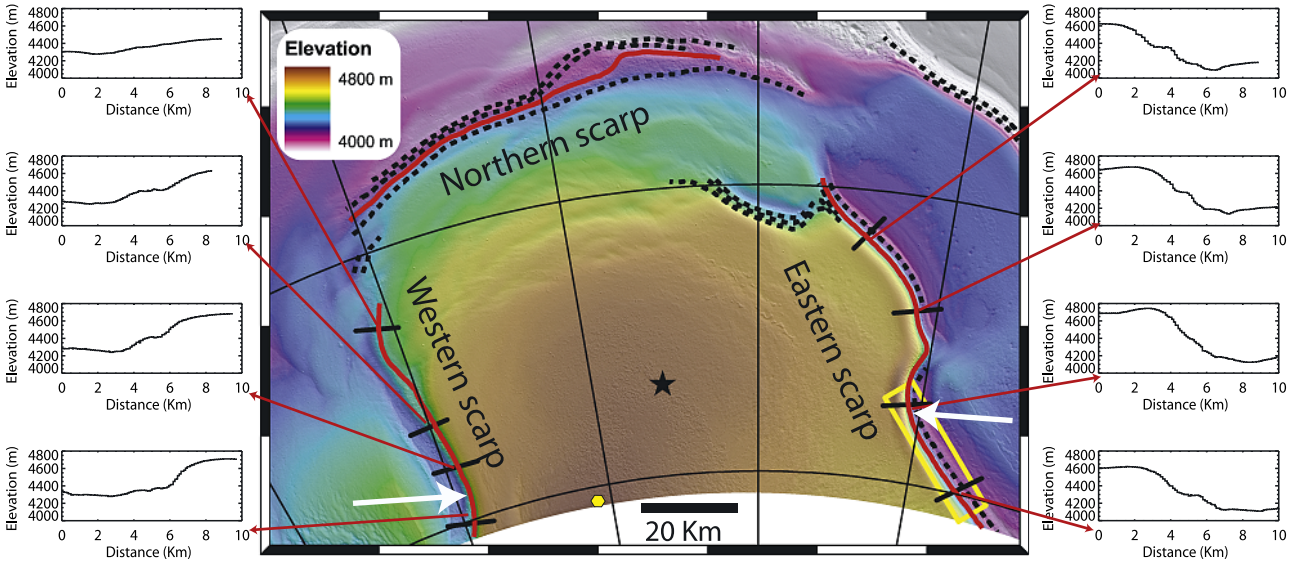

Figure 3. Annotated view of the topography of our initial study area, the location of which is shown in Figure 1. Parallels and meridians are plotted every 1° and 10°, respectively. This region is dominated by a large plateau bounded to the east, west, and north by indicated scarps. The southern border of this plateau is also bounded by a scarp, which is not shown due to a paucity of MOLA data poleward of 87°S, but which is discussed in section 4.4. Yellow rectangle at 87°S, 15°E indicates the position of Figure 4. Yellow hexagon at 87.3°S, 349°E indicates highest topographic point of the SPLD at 4799 m. The star at 86.6°S, 353°E indicates the highest point of the modeled interior surface discussed in section 3 at 4524 m (231 m below the topographic surface). Sample cross sections of the eastern and western scarps are shown. A prominent topographic bench can be seen in most but not all cases, illustrating the need for higher-resolution visible imagery in addition to topographic data. Bench-forming layers have been mapped as described in section 2.3 and are shown here by dashed lines. The red lines indicate those bench-forming layers that have been identified to be BFL_3 (see text) and which are used in the fitting of mathematical surfaces discussed in section 3. The white arrows indicate the location of frames shown in Figure 5. The profiles are taken from the 115 m/pixel DEM and have a vertical exaggeration of 5.

latitudes will be quoted in their aerographic form using the IAU 2000 ellipsoidal flattening.

2. Area and Techniques

2.1. Study Area and Data

[16] Our initial study area (Figure 3) encompasses the top tier of the stepped structure shown in Figure 1 over longitudes −20°E–15°E and latitudes 87°S–85.5°S. It is dominated by a central plateau which includes the highest portion of the SPLD (4800m). This plateau is bounded to the east and west by scarps of slope 10°–15° (the eastern scarp being systematically steeper). The plateau is bounded to the north by a shallower scarp of lower relief. The southern boundary is due to a paucity of spacecraft data poleward of 87°S. The flat areas of this study region are covered by residual CO_2 ice.

[17] Data coverage of this area has benefited immensely from the near-polar orbits of the MGS and Mars Odyssey spacecraft. Gridded elevation products are available from the MOLA team at resolutions as high as ∼115 m/pixel. Because of its unsurpassed accuracy, we have made the MOLA-derived digital elevation model (DEM) our basemap and registered all other data to it. The three scarps of interest to us, bounding this plateau, have near-complete coverage of high-resolution Mars Orbiter Camera (MOC) images (1.5–12 m/pixel) and complete coverage of lower-resolution Thermal Emission Imaging System visible (THEMIS VIS) images (18–36 m/pixel). Figure 4a illustrates the quality of the high-resolution images along a section of the eastern scarp. Unfortunately, due to the timing of polar traverses of MGS, many MOC images of west-facing scarps are over-saturated. However, there are still many usable images, especially those taken during polar twilight such as the M03, E05 or R05 mission phases.

[18] MOC and THEMIS VIS images were processed with the USGS ISIS software. These images were then carefully registered to the MOLA-derived DEM. When MOC images were simultaneously taken with MOLA data we use the location of those MOLA points to translate the projected image to a best-fit location on the DEM (described by *Byrne and Murray* [2002]). Positional errors after this step are of the order of 10–100 meters, consistent with positional uncertainties of individual MOLA shots reported by *Neumann et al.* [2001]. In all cases the final positioning of images relative to the DEM is manually undertaken. In contrast to the northern polar layered deposits, the SPLD appear rugged at the length scales of the MOLA DEM. Due to this effect there are many small-scale features that can be seen in both MOC images and shaded relief views of the MOLA DEM. We assume the MOLA data are essentially perfectly positioned so that these features can be used as control points to register MOC images. In general MOC images were only translated (using one control point) to

coincide with the DEM. On rare occasions the image was reprojected using an affine transformation constrained by many control points. Where an image had simultaneously acquired MOLA data, this manual correction was usually quite small (a few tens of meters); where simultaneous MOLA data were not available the correction was typically a few hundred meters. We estimate the final positional accuracy of the MOC images to be roughly one MOLA DEM pixel (115 meters) in an absolute sense. In a relative sense these images are registered to each other to within 10–20 meters.

[19] MOC images taken after mid-August 2001 are avoided when possible, as MGS had entered relay-16 mode. These images have emission angles of ~16°, so scarps and other sloping surfaces appear either extended or foreshortened (depending on viewing geometry). During this period, spacecraft pointing is also less reliable and no simultaneous MOLA data are available. Images may be mispositioned by over a kilometer relative to the MOLA DEM, making automatic orthorectification unfeasible. In future they may be corrected by manually controlling the original projection with points from the MOLA DEM.

2.2. Morphology of Scarps and Bench-Forming Layers

[20] The topography in Figure 3 and available imaging show a protruding flat bench on both the eastern and western scarps. Figure 4a illustrates the visible appearance of this feature on a section of the eastern scarp. In Figure 4b we show a morphological sketch map which names the major features discussed throughout this paper. Bench-forming layers are abbreviated to BFL, distinguished from each other by numerical subscripts. The main bench-forming layer on which we focus in this paper is BFL_3. It has been colored differently than other bench-forming layers shown in Figure 4.

[21] Layer sequences that have steeply sloping exposures are abbreviated to SS, again distinguished from each other by numerical subscripts. "Steep" refers only to the slope of their exposures not to their actual dips. Layers in these steeply sloping exposures appear thin in plan view; however, this is likely to be due to the steeper slope of the scarp at that location. It should be understood that descriptors such as "fine" or "thin" refer only to their appearance in plan view. These layers cannot be resolved by MOLA in the same way as the bench-forming layers; however, by dividing the relief of the stack by the number of layers, we estimate (to first order) that each layer has a thickness of ~10 m. Probable spatial variations mean that this number is only a rough guide. The layers in these steeply exposed sequences are

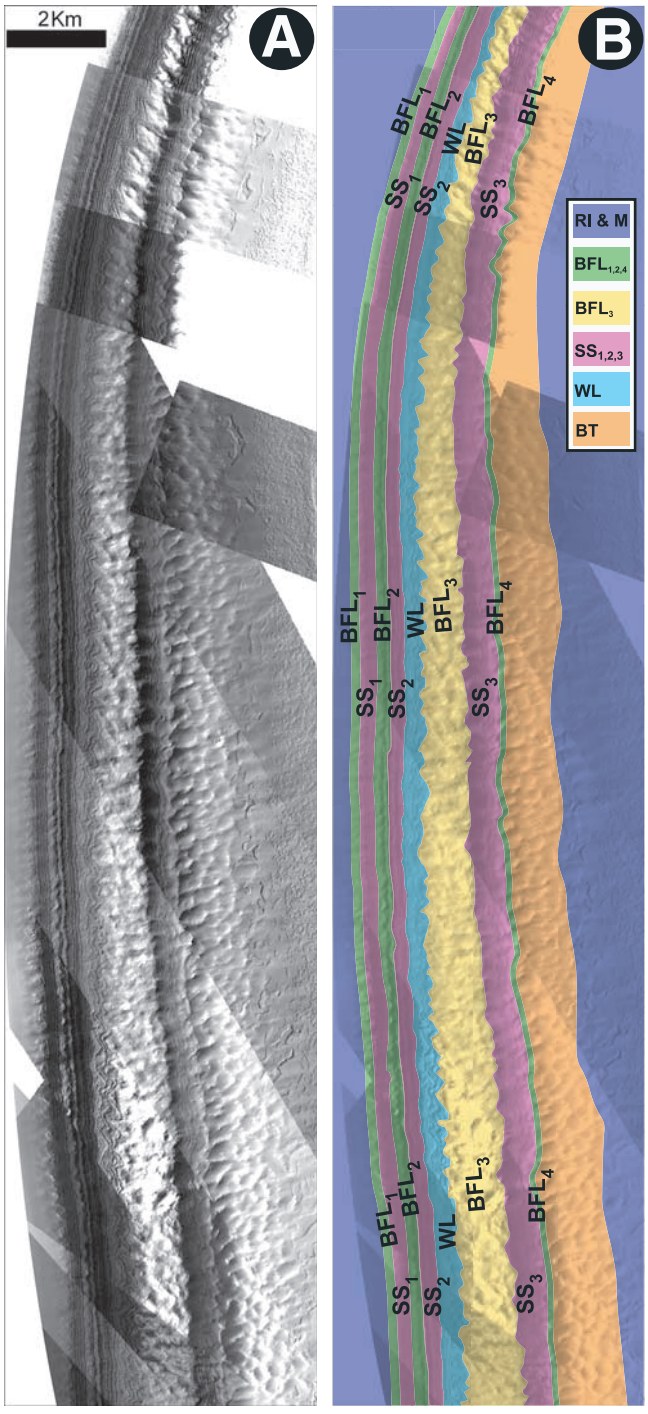

Figure 4. Portion of the eastern scarp (location indicated in Figure 3). Elevation decreases from left to right, and illumination is from the left. MOC imaging coverage (of which only a sample is shown) is particularly dense and of good quality here. The mapped bench-forming layer (BFL_3) protrudes prominently. Other resistant layers are marked as $BFL_{1,2,4}$; steeply exposed layer sequences are marked as $SS_{1,2,3}$. Layering visible above and below BFL_3 is continuous along the entire length of this scarp. Of interest is a prominent double layer (BFL_2). The "wavy" morphology of the layers (WL) directly above the bench-forming layer can also be seen here. Above and below the scarp the SPLD are covered with residual CO_2 ice (RI) and a cohesive low-inertia mantle (M). The "bowl-terrain" (BT) below BFL_4 is exposed all along the base of the eastern scarp. Each image in this mosaic was acquired at different seasons, spanning the entire portion of the Martian year for which daylight is available at this location. However, each image is either fully covered or fully free of seasonal CO_2 frost. See enhanced version of this figure in the HTML.

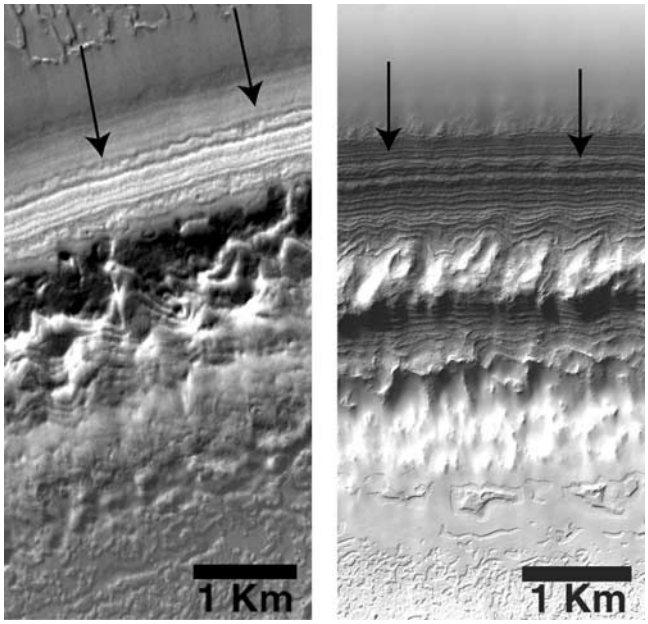

Figure 5. High-resolution MOC images of the western (M03/05143, L_s 178°, 13.5 m/pixel, on left) and eastern (M08/05817, L_s 230°, 2.8 m/pixel, on right) scarps of the study area. Elevation decreases from top to bottom in both cases, and illumination is from the bottom right and top left, respectively. Both scarps display a protruding bench-forming layer (BFL_3) with a series of finer layers both above (SS_1, SS_2) and below (SS_3). The relative position of a prominent double layer (BFL_2) indicated by arrows on both scarps confirms that the bench on each scarp is in fact formed by the same stratum. The positions of these two images are indicated by white arrows in Figure 3. See enhanced version of this figure in the HTML.

too similar to each other for them to be especially useful as stratigraphic markers.

[22] The protruding main bench (BFL_3) is heavily pitted and appears rough at diverse scales, both in the MOLA topography data (115 meters/pixel) and the MOC visible imagery (pixel sizes are typically a few meters and features a few times this size can be resolved). On the bench itself we see no evidence of contacts between layers in any of the images we have inspected. We interpret its surface to be therefore composed of one stratum. This implies that the dip of the layers is close to the bench-slope in these exposures. The bench surface may expose different levels within the BFL_3 stratum; however, it does not intersect the stratum directly below that.

[23] Lower in the stratigraphic sequence a second bench-forming layer (BFL_4) is visible; farther northward along the scarp it evolves into a topographic bench similar to BFL_3 with the same heavily pitted surface texture. BFL_4 is not exposed along the entire length of the scarp; its lower elevation means that it is below the current topographic surface in some locations. BFL_3 and BFL_4 are separated by a sequence of fine layers (SS_3). Close inspection of MOC images shows what appears to be BFL_3 overhanging SS_3. This is consistent with the situation described in section 1 where layers underneath a bench-forming stratum retreat faster and undercut it, leading to mass-wasting. The lack of debris at the base of the scarp (or indeed any of these scarps) could imply either a composition of clean ice or efficient removal of nonvolatiles by wind.

[24] The layers directly above the main bench (BFL_3) exhibit a "wavy" morphology (and are designated WL). They are in a transition zone between the bench (where surface slope is less than or nearly equal to the dip of the layers) and the rest of the scarp (where the surface slope is much greater than their dip). This "wavy" morphology may be a consequence of having a section of the exposing scarp that is almost parallel to the dip of the layers themselves. Small perturbations in layer elevations and thicknesses interacting with this exposing surface could result in large horizontal excursions of the exposure in plan view. Their appearance may then be a natural effect of the exposure geometry rather than due to actual folding of the layers themselves. However, we do not see this "wavy" morphology adjacent to other bench-forming layers elsewhere in the stratigraphic column so it may have some value as a stratigraphic marker.

[25] Stratigraphically above WL are two steeply exposed layer-sequences, SS_2 and SS_1. These are separated by two prominent neighboring layers (collectively designated by BFL_2). BFL_2 is easy to distinguish from the surrounding strata and we will make use of it as a stratigraphic marker throughout the paper. BFL_2 is immediately recognizable as both of its component layers protrude from the scarp and are immediately adjacent to each other. On the northern end of the eastern scarp BFL_2 widens in plan view to become a topographic bench similar to BFL_3.

[26] We interpret the sharp break in slope at the top of the scarp to be also caused by a resistant layer which we designate BFL_1. Above and below the scarp, the layered deposits are obscured by residual CO_2 ice (RI) and the cohesive mantle (M) described in section 1 and found throughout the SPLD. Below BFL_4 is an unusual terrain of bowl shaped depressions (BT), which may be sun cups formed by solar erosion of H_2O ice [Ken Herkenhoff, USGS, personal communication].

[27] The bench-forming layer observed by *Herkenhoff and Murray* [1990b] corresponds to BFL_3 on the eastern scarp. Using photoclinometry of Mariner 9 imagery, the authors retrieved thickness and surface slopes for the upper (SS_2 + BFL_2 + SS_1) and lower (SS_3) finely layered sequences. Due to the limited image resolution, they treated each of these sequences as an individual layer. Their three retrieved elevation profiles agree closely with the MOLA data presented here.

[28] Figure 5 shows a close view of the benches on both the eastern and western scarps. Both exposures show a flat protruding bench with a rough pitted appearance (interpreted to be BFL_3). They both show steeply exposed sequences of layers above and below the protruding bench. In the sequence of strata above the bench, a prominent double layer (indicated by arrows on Figure 5) can be seen in both cases (interpreted to be BFL_2). These stratigraphic and morphologic similarities show that these two benches, on the eastern and western scarps, do indeed correspond to the same stratigraphic surface (BFL_3). Each bench can be mapped for tens of kilometers along these scarps. The red lines along these scarps in Figure 3 show where we have mapped the surfaces of these topographic benches. The

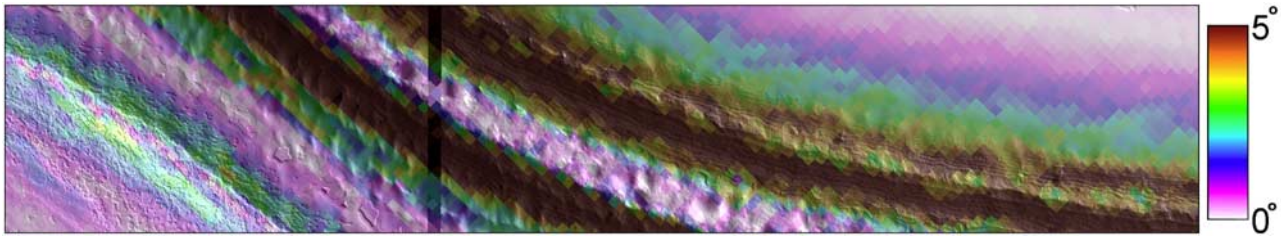

Figure 6. Combination of downhill slope derived from a MOLA DEM with MOC narrow angle M07/01348 (L_s 202°) for shading (illuminated from the top right). The bench-forming layer, BFL_3, shows up prominently as a strip of extremely low slope with the sloping scarp both above and below (elevation decreases from top right to bottom left). Although the color scale saturates at 5°, steeper parts of the scarp can reach 15° in this area. The prominent double layer, BFL_2, also shows up as a shallower region within the upper part of the scarp. Combining data sources in this way makes the mapping process more reliable. The downhill slope on the bench itself is only a fraction of a degree, consistent with the dips of the model surface calculated in section 3. This comparison lends support to the observation that the bench surface is composed of a single layer. A thin strip of missing MOC data can be seen just to the left of center. This figure is 2.8 km high. See enhanced version of this figure in the HTML.

topographic bench (due to BFL_3) is wider on the western scarp than on the eastern, indicating that more retreat of the overlying layers (SS_2 + BFL_2 + SS_1) has taken place in that location.

[29] To the north of the central plateau there are few distinct scarps except for the final bounding scarp of the layered deposits (at 84°S–85°S). Between this scarp and the central plateau the SPLD have many low-relief, shallow exposures. This topography contrasts with the handful of high-relief, steep scarps to the east and west of the initial study area. The lower slope of the northern scarp, which bounds the central plateau, results in several layers forming benches. This area also has a smooth mantling deposit which, in places, buries the scarp containing BFL_3. This mantle means the northern exposure of this bench-forming layer is not connected to the eastern or western exposures. A careful examination of MOC images, topographic profiles and 3-D perspective views helps us distinguish which of the benches on this northern scarp is formed by BFL_3. We will describe in section 3 how later surface fitting validated this choice. The red line along the northern scarp in Figure 3 shows where we have mapped the surface of BFL_3 in that location.

2.3. Measurements of Bench-Forming Layers

[30] Once bench-forming layers were identified we mapped their exposures using high-resolution MOC frames and MOLA topographic products. THEMIS VIS frames were used as a consistency check. All data were assembled and viewed in a geographic information system (Arcmap by ESRI) using a polar stereographic projection. This system allows us to easily switch between visible and topographic data sets, view maps at a variety of scales and in three dimensions if needed.

[31] Shaded relief products and slope maps derived from MOLA topography are especially useful in identifying the exact location of protruding flat benches. These features can continue to be mapped through gaps in imaging coverage using these products. Figure 6 shows an example of a representative portion of the eastern scarp. The high-resolution imagery and lower-resolution slope measurements can be combined as shown. Including the slope derived from the DEM in this combined analysis is extremely useful as it is the DEM from which we will extract the elevation points.

[32] Once the features have been mapped in this system it is relatively easy to extract the position and elevation of each point. The elevation is calculated from the 115 m/pixel DEM using bilinear interpolation of the surrounding four pixels. The x and y locations are given as meters in a polar stereographic projection with (0, 0) at the south pole and the positive y-axis on zero longitude. The result of this analysis is a set of measurements of the position of the top of the bench in three dimensions.

[33] The top of any one stratum is a paleosurface or "isochrone" of the SPLD. Even though the surface of this bench does not intersect more than one layer it may not necessarily represent the top of BFL_3. As mentioned in the previous section, layers in the steeply exposed sequences on the eastern scarp appear to be roughly 10 m thick. The thickness of BFL_3 may also be close to this average value; however, given its resistant nature it may be thicker. Different levels within BFL_3 may be exposed at different places along the bench as the bench surface is rough. Although the top of BFL_3 represents a distinct stratigraphic horizon or paleosurface of the layered deposits, the surface of the bench itself is only an approximate paleosurface since the material it exposes has been deposited over whatever length of time it took to form that layer.

[34] The heavy red lines on Figure 3 indicate the mapped exposures of BFL_3. Heavy dashed black lines indicate other bench-forming layers which correspond to different strata. The three-dimensional points we have collected of BFL_3 will be examined in detail in the next section. They are concentrated along three distinct exposures on the eastern, western and northern scarps. These exposures are not contiguous, as noted above. The exposures on the eastern and western scarps are mapped as far south as possible. Due to a paucity of spacecraft data they cannot be mapped farther southward than a latitude of 87°S.

3. Polynomial Fits of Bench-Forming Layers

[35] The measurements of the three-dimensional location of BFL_3 are irregularly distributed (being only available

Table 1. Coefficients of Surface Fits and Standard Deviations of Residuals[a]

Order	a_0	$a_1 \times 10^3$	$a_2 \times 10^3$	$a_3 \times 10^8$	$a_4 \times 10^8$	$a_5 \times 10^{13}$	$a_6 \times 10^{13}$	$a_7 \times 10^{19}$	$a_8 \times 10^{19}$	σ, m
0th	4312.84	≡0	≡0	≡0	≡0	≡0	≡0	≡0	≡0	93.62
1st	4823.09	0.2501	−2.351	≡0	≡0	≡0	≡0	≡0	≡0	57.79
2nd	1079.08	−1.86	34.7	−4.67	−8.80	≡0	≡0	≡0	≡0	11.71
3rd	65.83	−2.15	47.4	−3.51	−14.0	1.86	0.707	≡0	≡0	10.66
4th	32747.37	−2.54	−573.0	−3.05	424.0	3.63	−135.0	7.52	157.0	7.64

[a]≡0 indicates that coefficient not needed for that surface.

where there happens to be an exposure). There are about 260 individual points in total. We investigate this surface by attempting to fit planes and surfaces with low-order curvature to these measurements using linear regression techniques. The mathematical form of these surfaces is a simple polynomial shown in equation (1). Cross terms are not included. The number of free parameters increases with the complexity of the model surface, equaling $2n + 1$ where n is the order of the polynomial. For example a 0th-order surface is a horizontal plane and has only one free parameter which is the elevation of that plane. A 1st-order surface is an inclined plane and includes an elevation and independent tilting in the x and y directions (3 free parameters). A 2nd-order surface is parabolic and includes all the 1st-order terms in addition to independent curvature in the x and y directions (5 free parameters). Higher-order surfaces give more complex behavior. The best-fit coefficients derived for these surfaces are shown in Table 1.

$$z = a_0 + \sum_{p=1}^{n} \left(a_{[2p-1]} x^p + a_{[2p]} y^p \right). \quad (1)$$

[36] To determine the quality of each model surface we evaluate the differences between the actual heights and modeled heights of each mapped point. We use the standard deviation of these residuals as a measure of how accurately each fitted function describes the data. Since the coefficients of these functions are the "best-fit" values the mean of the residuals is always zero. Standard deviations of residuals for each model surface are shown in Table 1 and Figure 7a. The simplest solutions, i.e., those of a horizontal (n = 0) or inclined (n = 1) planar surface yielded unacceptably large residuals. A 2nd-order surface (parabolic dome) however yielded an excellent approximation to the measurements (the standard deviation of the residuals being only 11.7 meters). Higher-order surfaces yield (as expected when additional free parameters are introduced) small improvements in the magnitude of the residuals, however these improvements are modest compared with those previously seen. We feel that we are simply hiding noise within these additional free parameters and that the 2nd-order surface describes these data adequately. For the rest of this paper we use this 2nd-order surface to describe the shape of BFL_3.

[37] The central location (apex) of this 2nd-order model surface can be retrieved from the fit coefficients. It is offset from the origin (x = y = 0, south pole) and is given by equations (2) and (3).

$$x_c = \frac{-a_1}{2a_3}, \quad (2)$$

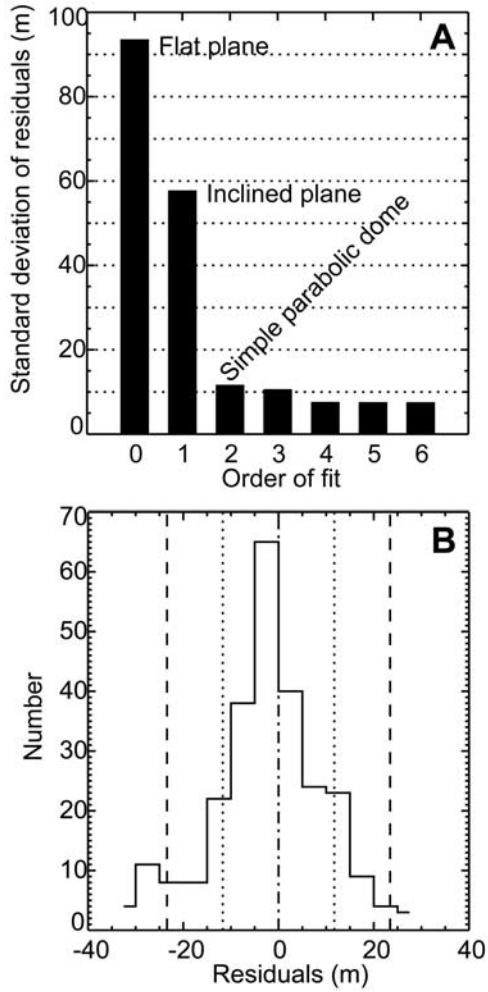

Figure 7. (a) Standard deviations of residuals for various fits to the data. Dramatic improvements in the quality of the fits are visible as one progresses from a horizontal plane (1 free parameter) to an inclined plane (3 free parameters) and from there to a surface with both an inclination and curvature (5 free parameters). Higher-order surfaces with more free parameters show only minor improvements in the magnitude of the residuals. (b) Histogram of residuals between the 2nd-order surface and the mapped data. First and second standard deviations are indicated by the dotted and dashed vertical lines, respectively. More than 90% of the 259 data points fall within 21.5 vertical meters of this model surface, which contains only 5 free parameters. The data were originally spread over ~330 m vertically.

$$y_c = \frac{-a_2}{2a_4}, \tag{3}$$

$$Dip = \arctan\left(\sqrt{(a_1 + 2a_3x)^2 + (a_2 + 2a_4y)^2}\right). \tag{4}$$

[38] Cartesian coordinates can be converted back to longitude and latitude using the inverse formulas for a polar stereographic projection [*Snyder*, 1987]. The location of the apex of this surface is indicated by the star on Figure 3 at 86.6747°S, 354.2316°E, which is roughly 27 km from the highest topographic point of the SPLD. The maximum height of this surface is 4524 m, which at that location is 231 m below the surface topography. The dip of the layers (evaluated from $\arctan|\nabla z|$; see equation (4)) at the exposures where the data points were taken is very low, with mean downhill slopes of 0.30°, 0.35° and 0.60° on the western, eastern and northern scarps, respectively. This is close to the dip observed on the benches themselves (see Figure 6 for example). Since the bench has the same dip as is inferred for the layers it is expected to intersect only one stratum. This is consistent with our observation that the surface of the bench is composed of only one layer. This model surface decreases in elevation and increases in downhill slope with distance from its apex. Since this is only a 2nd-order surface there are no reversals in slope except at the apex itself.

[39] Figure 7b shows the histogram of residuals for this 2nd-order surface. This simple model describes the shape of BFL_3 with remarkable accuracy: 90% of the mapped data points are within 21.5 meters of the surface despite the fact that they are spread over tens of kilometers laterally and hundreds of meters vertically. For comparison, the average layer thickness determined in section 2.2 was $\sim$10 m.

[40] As discussed in section 2.2, the bench which we mapped along the northern scarp was chosen on the basis of an aggregate examination of available data. However, in this area there are several topographic benches due to the lower slope of the exposure. To confirm that we had chosen the correct bench to map we tested those neighboring benches. Data from each topographic bench were included in turn in the solution of the best-fit surface. We examined the quality of the fit to the data for each possible bench on this northern scarp and found our initial choice gave the best results (i.e., lowest residuals).

[41] When the correct data points from this northern scarp are used in the fit the coefficients of the model surface do not change appreciably and the standard deviation of the residuals increases by only $\sim$0.5 m. The three-dimensional position of this northern exposure is thus already well constrained just from the data taken on the eastern and western scarps.

[42] MOLA is an exceptionally accurate instrument and errors in its height measurements are negligible (<1 m) [*Neumann et al.*, 2001] compared with the standard deviation of our residuals. The source of these residuals is rather due to the nature of the surface being investigated. These benches are heavily pitted. These pits are not fully resolved by the MOLA DEM; however, we can estimate their depth by examining a detrended elevation profile taken along the surface of the bench. The amplitude of the topography in such a profile is an indication of the relief of the pits. We find this amplitude to be in the range of 10–20 meters. These pits are likely to be an important source of topographic noise at this scale. The stratigraphic surface of BFL_3 is therefore likely to be even more closely approximated by this model surface than the current residuals imply.

4. Extending to Lower Scarps

[43] Given the shape of this model surface, it is possible that it intersects the topography in locations other than where BFL_3 was originally mapped. We are now in a position to use this model surface to predict where other outcrops of BFL_3 exist. We can subtract this model surface from the actual topography to find where these two surfaces intersect. Figure 8 shows a wider area with colored regions indicating where the model surface is above the topography and gray where it is below the topography. The closed polygons that form the boundaries of these colored regions indicate locations where this model surface is predicted to intersect the topography. The bench-forming layer BFL_3 should therefore be exposed at these boundaries. These model-predicted exposures (MPEs) occur both on scarps and on the intervening flat surfaces.

[44] Layering is generally not exposed on these flat surfaces. They are covered by either the few meters of CO_2 ice which comprise the residual cap or the cohesive mantling deposit that covers other areas on the layered deposits. Even if these obscuring deposits were absent it would likely be difficult to recognize sequences of layering on flat topography. Individual layers would be extremely extended in plan view since the surface slope is close to the dip of the layers. If the scarps have migrated poleward by some amount then it is possible that this ablated material may be redeposited on the flat interscarp areas, as first suggested by *Howard* [1978]. These flat areas may therefore be capped by horizontal layers which have been much more recently deposited (see Figure 9). This deposition would further obscure the original stratigraphy over flat interscarp areas. Figure 9 illustrates our expectations of strata geometry near scarps. If this geometry is correct then a buried angular unconformity between these recent horizontal layers and the original dipping layers may be present. Unfortunately, such an unconformity could only be seen in an exposure perpendicular to the scarps (which does not exist); however, future radar sounders may be used to test for its presence.

[45] On the basis of Figure 8 we would expect to find this bench-forming layer (BFL_3) exposed on several scarps where we have not yet mapped it (indicated by N1, E2, W3, etc.). The validity of this model surface as a description of this internal stratum can be tested by looking for exposures of BFL_3 at these model-predicted locations (MPEs). In the following subsections we show evidence that this layer has outcrops at the MPEs discussed above. We defer a discussion of the color coding in Figure 8 until after these predicted exposures have been verified below. In the following subsections we show evidence that BFL_3 does crop out at the MPEs to the north, south, east and west of the original study area.

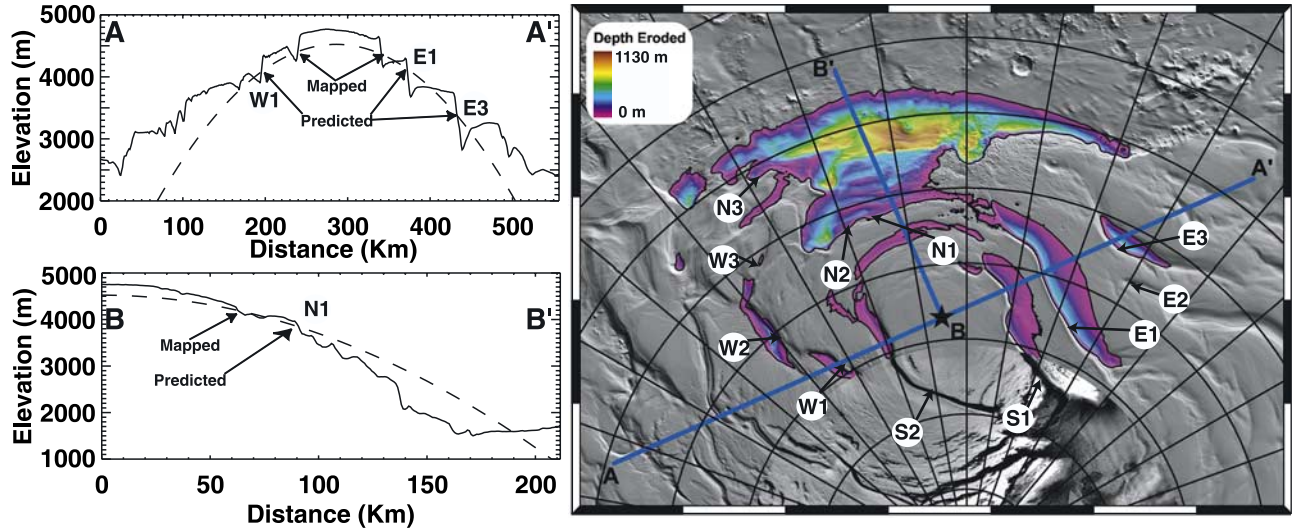

Figure 8. Locations of model-predicted exposures. Right panel shows where (and by how much) the model surface is above the current topography. Locations where the model surface is below the topography have no color. The edges of the colored regions mark the MPEs of BFL_3. Background shading is a combination of MOLA shaded topography and MDIM 2.1 (a Viking image mosaic produced by the USGS) within ~87°S. Star symbol indicates location of highest point of the model surface. The cross sections AA′ (vertical exaggeration of 75) and BB′ (vertical exaggeration of 22.5) are shown in the left panels, where actual topography is plotted as a solid line and the model surface is plotted as a dashed line. Mapped and model-predicted exposures are indicated. The location of confirming visible imagery shown in subsequent figures is given in the right panel, labeled as "N1," "W3," etc. See enhanced version of this figure in the HTML.

4.1. Verifying Predicted Exposures to the West

[46] Figure 8 shows MPEs of the bench-forming layer BFL_3 on scarps located to the west of the original study area. Figure 10 shows MOC images from each of those locations (marked as W1, W2 and W3). In each case the bench-forming layer, BFL_3, has an outcrop at or close to the expected location (indicated by the heavy black line). In some cases the prominent double layer (BFL_2), seen above BFL_3 on the originally mapped eastern and western scarps, is visible and indicated by arrows.

[47] In the case of the scarp at W1 the mean offset between the MPE and the observed bench is only 7.3 meters. It is remarkable that although this exposure is over 100 km from the inferred center of the deposit, its position can be predicted so accurately. The dips of the layers, inferred from our model surface (see equation (4)), have increased to an average of 0.6°. The surrounding stratigraphy, especially the prominent double layer, BFL_2, indicated by arrows in Figure 10 confirms this bench is the same stratum that we have originally mapped (BFL_3).

[48] The scarp at W2 presents a more complicated story. The MPE of BFL_3 coincides exactly with a bench in that scarp (with a similar mean offset as W1). However the layering here is poorly imaged (due to low image resolution and poor atmospheric and lighting conditions) and has a disrupted appearance (Figure 10). There is another bench-forming layer above the MPE that could possibly be BFL_3. If this were the case then the mean offset between the bench and prediction would be 156 meters. However, we interpret this higher bench-forming layer to be BFL_2 (see Figure 4) and not the main stratum which we are investigating. At this

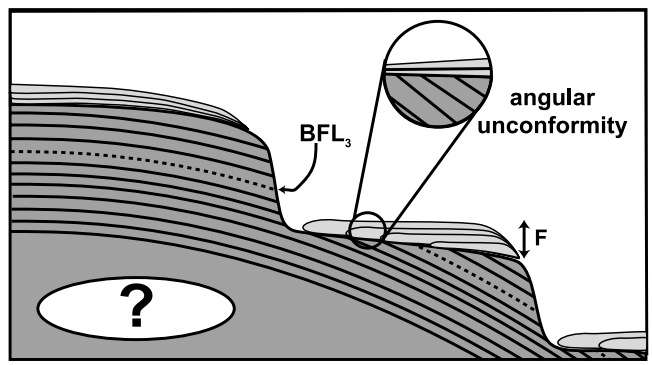

Figure 9. Cartoon cross section showing layering geometry in the vicinity of scarps. Retreat of the scarps has exposed the internal curved layering of the SPLD, which includes BFL_3. Layer sequences repeat from scarp to scarp. Since this study applies to the upper few hundred meters, the interior layering is unconstrained. Material ablated from the retreating scarps may be deposited on the expanding interscarp flat areas. This material (F) can cap the flat areas with fresh horizontally bedded layers. Alternatively this flat lying material may not be layered if the ratio of volatiles to nonvolatiles has not changed during the period of its deposition. These flat areas are also buried by a cohesive mantling deposit (as discussed in section 1). The buried angular unconformity may be observed in the future by surface-penetrating radar.

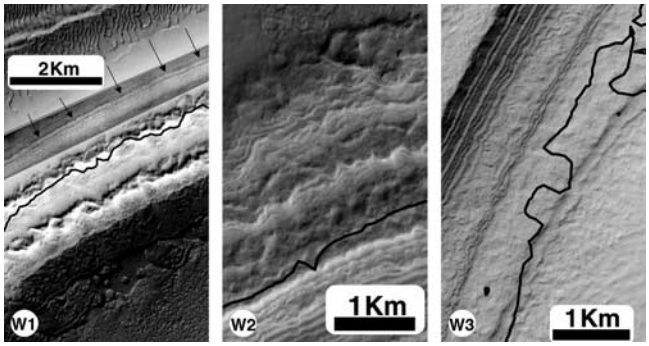

Figure 10. MOC high-resolution views of MPEs of BFL_3 to the west of the initial study area. The heavy black line denotes exactly where the model surface intersects the topography. The positions of subframes W1 (M03/04417, L_s 175° and E05/01416, L_s 180°), W2 (M03/04191, L_s 175°), and W3 (M09/02772, L_s 242°) are all indicated in Figure 8 and are illuminated from the bottom right except for W3 (illuminated from top). Note part of the image W1 has been locally stretched so that the layering is visible; the prominent double layer (BFL_2) is again visible here (shown by arrows). Elevation decreases from top to bottom in all cases. See enhanced version of this figure in the HTML.

location the dip of our model surface has increased to an average of 0.7°.

[49] The scarp at W3 is almost continuous with the scarp containing W2. Here the MPE lies exactly on a bench-forming layer. We infer that this is the correct stratum (BFL_3) on the basis of the set of "wavy" layers (WL in Figure 4) that are immediately stratigraphically above it. We cannot rule out the possibility that this "wavy" morphology may just be a natural consequence of this bench-and-scarp topography (as discussed in section 2.2). However, as previously noted, the fact that it is not associated with all benches gives us some confidence that it can be relied on as a stratigraphic marker.

[50] MPEs of BFL_3 agree well with observations in this region, west of the original study area.

4.2. Verifying Predicted Exposures to the East

[51] Figure 8 shows MPEs at several locations to the east of the original study area. Figure 11 shows MOC and THEMIS images from each of those locations (marked as E1, E2 and E3). In each case except one, BFL_3 has an outcrop at or close to the expected location (indicated by the heavy black line). This exception can be explained and will be discussed below.

[52] For the scarp at E1 the mean vertical offset between the MPE and the bench itself is only 5.1 meters. This exposure spans a large distance (being 133 km long); its distance from the center of the deposit ranges from 84 to 136 km. Yet this method can accurately predict its mean location to within a few meters. In this location the dips of the layers, inferred from our model, have increased to an average of 0.6°. The surrounding stratigraphy confirms this bench corresponds to BFL_3.

[53] In this case, although the mean offset of the MPE from the bench is small, the actual offset varies widely over the length of this scarp, being low at the northern and southern extremes and high in the middle. Despite the fact that the prediction is good overall, the standard deviations of the elevation offsets between the observed exposure and MPE are large (~81 m). We will discuss the reason behind this at the end of this section.

[54] The MPE at E2 is not at a steep scarp, but is at the beginning of a gentle trough. It forms a closed contour at the bottom of this trough. Here BFL_3 is expected to be barely above the surface, indeed at the scale of Figure 8 it is difficult to even see that this area is colored. Within this trough a heavily pitted surface resembling that of BFL_3 is exposed. The topography in this location does not expose any strata below this. Above this pitted layer, the walls of the trough appear mantled so that layering is difficult to observe. Thus the only evidence we have of BFL_3 at this location comes from its similar surface texture. This observation is consistent with the proposed model but does not offer strong confirmation.

[55] The MPE at E3 lands close to a bench-forming layer; however, the mean vertical offset from that layer is 95 m. There is another candidate bench-forming layer farther up that scarp, with a mean vertical offset from the MPE of 187 m. We interpret this higher topographic bench to be what was observed as the prominent double layer (BFL_2) on the original scarps (see Figure 4). We interpret the lower bench-forming layer (still 95 vertical meters away from the MPE) to be the correct stratum, BFL_3. The vertical offset of this lower bench (BFL_3) from the MPE ranges from 6 m to 180 m at different points along the length of this exposure. Clearly, a mean offset of 95 m is a large error and indicates that this approach is breaking down in this area. One suspects that a parabolic function is simply no longer suitable to describe this stratum in this area; however, the abruptness of the transition from success to failure makes this difficult to understand. In this location the dips of the layers, inferred from our model surface, have increased to an average of 0.96°.

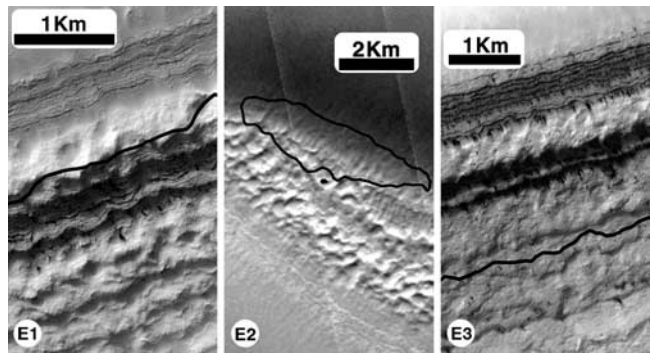

Figure 11. MOC and THEMIS VIS views of MPEs of BFL_3 to the east of the initial study area. The heavy black line denotes exactly where the model surface intersects the topography. The positions of subframes E1 (M08/02843, L_s 224°), E2 (V06202006, L_s 182°), and E3 (E08/00297, L_s 227°) are indicated in Figure 8 and are all illuminated from the top. Elevation decreases from top to bottom in all cases except E2, where elevation decreases toward the center from both directions. See enhanced version of this figure in the HTML.

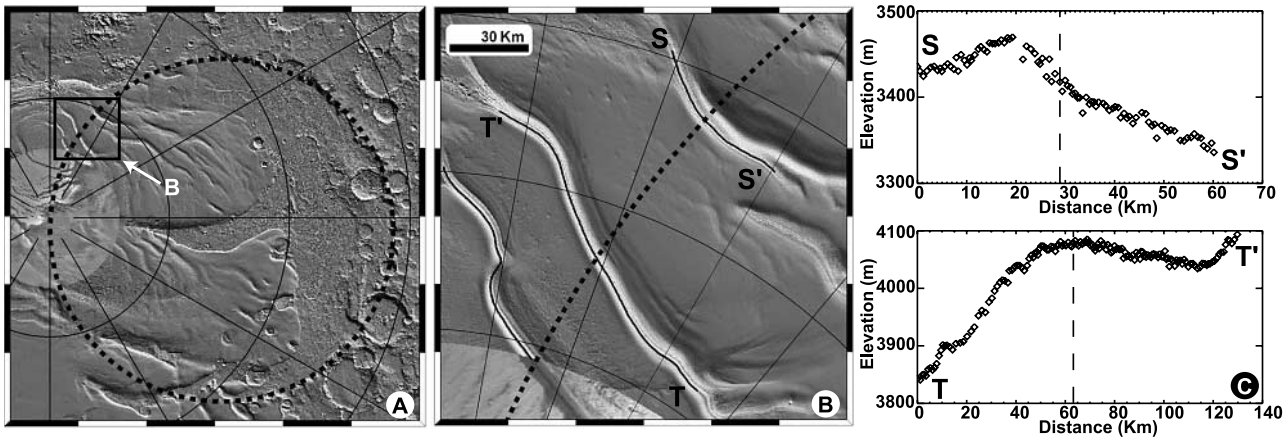

Figure 12. MOLA shaded topographic views of the relationship between the extrapolated edge of the Prometheus impact basin and mapped exposures of BFL_3 at E1 and E3. Figure 12a shows the regional context with the basin edge indicated by a dashed line. The position of Figure 12b is shown by the box in the top left. The size of the circle used to represent the basin is 857 km (centered at 82.8°S, 94.2°E). Figure 12b shows the area where the exposures TT′ (E1) and SS′ (E3) intersect the Prometheus extrapolation. The elevations along SS′ and TT′ are plotted in Figure 12c. The dashed vertical lines here show where the exposures intersect the extrapolated location of the edge of the Prometheus impact basin. Turnovers in these elevation profiles at or near the basin edge may indicate that basal topography is influencing the shape of the internal strata. See enhanced version of this figure in the HTML.

[56] One explanation for large standard deviations (E1) and large mean offset (E3) of the MPEs from the observed exposures is suggested by examination of the topography along each exposure. The elevations along the trace of BFL_3 at E1 (TT′) and E3 (SS′) are shown in Figure 12c. These elevation traces appear to turnover (i.e., reverse in slope) at specific locations not predicted by the model surface, causing significant error. Also shown on Figure 12 is the extrapolated location of the edge of the Prometheus impact basin, which is partly buried by the SPLD. The locations of these elevation turnovers (slope reversals) correlate closely with the extrapolated location of this feature.

[57] It seems likely that the basal topography has considerable relief at this location. We estimate the relief across the edge of the Prometheus basin in this location to be ~0.8–0.9 km. This estimate is based on actual measurements of the relief across the basin edge at a representative nearby section (at ~79.5°S, 50°E). This representative section was chosen for its undisturbed character and lack of any superposed later impacts. We suggest that the shape of the internal strata has been affected by basal topography. The implications of this are discussed in section 6.

4.3. Verifying Predicted Exposures to the North

[58] The terrain to the north of the original study area is severely disrupted by the M^{c}Murdo secondary crater field and identification of BFL_3 is less certain. In addition, the stair step structure of the layered deposits, which dominates to the east and west, is less pronounced here. Outcrops are generally located on low-relief shallow slopes with no more than a few layers being exposed in any one outcrop.

[59] This topographic expression means there are many layers which form benches even though these layers would not ordinarily do so on other, steeper, scarps. Likewise, the stratigraphic features which we use in the previous sections have also changed in appearance due to this different environment.

[60] Figure 8 shows several MPEs to the north of the initially mapped area. Some sample MOC narrow angles are shown in Figure 13 for the locations N1, N2, and N3. In general the MPEs all correspond with a bench-forming layer. Identification of these benches as BFL_3 is difficult. The different appearance of the surrounding strata rules out using them to make a definitive identification. The exposures of benches at N1 and N2 have a similar pitted texture as BFL_3 (see Figure 4). All three locations show a second bench-forming layer at lower elevation, which we interpret to be the one mapped as BFL_4 in Figure 4.

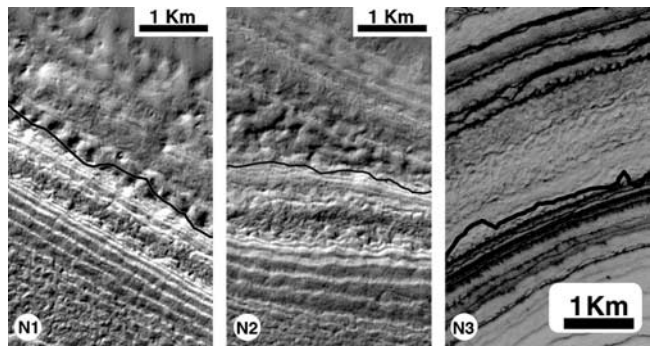

Figure 13. MOC high-resolution views of MPEs of BFL_3 to the north of the initial study area. The heavy black line denotes exactly where the model surface intersects the topography. The positions of subframes N1 (M03/03591, L_s 173°), N2 (M03/03128, L_s 172°), and N3 (E10/01170, L_s 268°) are indicated in Figure 8 and are all illuminated from the bottom right except for N3 (illuminated from top). Elevation decreases from top to bottom in all cases. See enhanced version of this figure in the HTML.

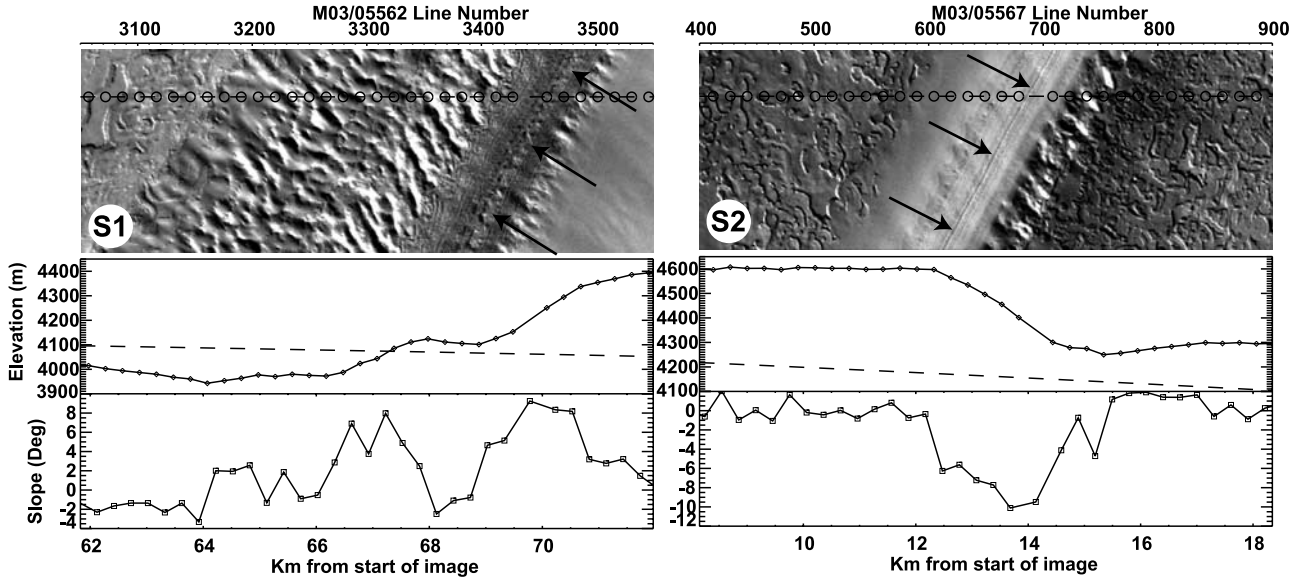

Figure 14. Confirmation of bench-forming layer BFL_3 close to its modeled location to the south of the original study area. Simultaneously acquired MOC and MOLA data for S1 (M03/05562, L_s 178°, illuminated from upper right) and S2 (M03/05567, L_s 178°, illuminated from upper right). Imaging and MOLA data are particularly badly positioned in the region poleward of 87°S since all data collected in this region are taken at a high emission angle. However, simultaneous data can be accurately tied together in a relative sense using their common acquisition times. Arrows indicate the prominent double layer, BFL_2, above BFL_3 in both cases. Circles indicate the size and position of individual MOLA shots. The solid lines plotted are the MOLA elevation (vertical exaggeration ~5) and slope data, and the dashed lines are the elevations of the model surface along that same profile. See text for discussion of offsets between the modeled and observed exposures. See enhanced version of this figure in the HTML.

[61] A definitive confirmation of the model is difficult to make in this region. The exposures observed above are all consistent with the proposed model.

4.4. Verifying Predicted Exposures to the South

[62] Testing for exposures of this surface to the south of the original study area is more problematic. Poleward of 87°S topographic and imaging data are sparse. To compound matters, the locations of data in this region are often poorly known since they were acquired at high emission angles. There are approximately 101 off-nadir MOLA tracks which cross some portion of this region giving about 97,000 topographic measurements. The paucity of topographic data (~80 times less than the surrounding DEM), coupled with poor positioning, makes generating an accurate DEM of this area unfeasible. Instead we test each MOLA track individually to see if it intersects the model surface.

[63] We find intersections with this surface in several tracks but only along two scarps. These locations are shown on Figure 8 (S1 and S2). A background context image (Viking MDIM 2.1, provided by the USGS) shows these locations to be on scarps that are continuations of the original eastern and western bounding scarps of the central plateau (see Figure 3). Figure 14 shows two MOC images displaying the bench-forming layer, BFL_3, where it was predicted in locations marked as S1 and S2 (see Figure 8). Surrounding stratigraphy such as the prominent double layer (BFL_2 in Figure 4) indicated by arrows confirms the bench is formed by the correct stratum, BFL_3. The MOLA data simultaneously acquired with these images are also shown (solid profile). The elevation of the model surface is shown as a dashed line. The vertical and horizontal positions of these data are poorly known in an absolute sense. However, the simultaneous MOC and MOLA data can be precisely co-located relative to each other as they share the same spacecraft clock.

[64] There are substantial vertical offsets between the model surface and the position of the bench (which we have identified as BFL_3). Assuming that the data are well positioned, they are 35 m and 129 m for S1 and S2, respectively. However, positional errors could also explain the offset between the model surface and observations. We have estimated the horizontal shift necessary to move the data into agreement with the model by using dips from the model surface (0.61°, S1 and 0.66°, S2). These shifts are ~3 km (S1) and ~11 km (S2). In fact, the data are likely to be mispositioned vertically as well as horizontally. The unusually large magnitudes of these errors are not unexpected within this region, for the reasons outlined above. In addition S1 is close to the extrapolated rim of the Prometheus basin (see Figure 12) and its position may be affected in a similar way to that discussed in section 4.2.

[65] In effect then, the model surface agrees with the observed location of the exposure within the accuracy of the data.

4.5. Scarp Erosion and Material Removed

[66] The model surface describes the 3-D shape of BFL_3 over a large area with predicted and confirmed exposures up to 160 km from its apex and in all directions. In general the model surface works best in the regions east and west of the

original study area. The exposures to the north and south of the original study area all are consistent with this model surface but for differing reasons do not offer strong confirmation (see previous subsections). Since exposures of BFL_3 are now known to span several scarps an immediate implication is that the scarps were created after this layer (and indeed several hundred meters of layered material above it) had been laid down.

[67] This fact rules out some of the mechanisms for scarp formation discussed in section 1. Scarps are not constructional features such as caused by thrust faults, since exposures would then not be expected to conform to a single dome-shaped surface. Other constructional methods such as depositing flat "plates" [*Murray et al.*, 1972] with gradually reduced extents are also inconsistent with these results. Similarly, ice-flow processes seem unlikely to be responsible for either their origin or modification. Flowing layers would be distorted in shape in the vicinity of scarps [*Fisher*, 2000; *Hvidberg*, 2003] which is inconsistent with the predictive ability of the simple function discussed in section 3. However, ice flow may be playing an active role in the modification of the troughs in the northern polar layered deposits [*Hvidberg*, 2003; *Fisher*, 1993; *Greve*, 2000]. The main candidate for the scarp formation mechanism is still ablation by solar radiation [*Howard*, 1978; *Thomas et al.*, 1992], perhaps aided by eolian activity [*Cutts*, 1973b; *Howard*, 2000].

[68] Martian polar scarps could possibly migrate poleward by ablation of their steep equatorward face and redeposition on the intervening flat areas as originally discussed by *Howard* [1978] (see Figure 9). Such poleward migration would effectively remove the original dipping stratigraphy and rework this material into flat-lying layers between scarps. We observe the same stratigraphy on many scarps, which indicates that they are still exposing the original stratigraphy of the SPLD.

[69] One interesting exercise is to try and estimate how far these scarps have migrated. We assume that the scarps retreat horizontally into the SPLD (which would imply they get higher as they retreat). We also assume that the SPLD have not been reduced much in height so the surface of the current central plateau represents the surface of the SPLD before scarp formation. The current topography of the central plateau is ~230 m above the highest point of BFL_3 (see Figure 8). We can assume that before it was disrupted by the formation of scarps that the surface topography followed the shape of BFL_3 with this constant offset. Using these assumptions we can reconstruct the original surface and so see how far scarps have retreated. In the case of the eastern bounding scarp of the central plateau this distance is 50 km. Since there are so many assumptions involved in this calculation this number should only be used as a rough guide.

[70] The regions of the model surface that are above the current topography are color coded in Figure 8 to show how far above the current topography they are. If this layer is assumed to have been continuous over these areas initially, then at least this much material has been removed by erosion during scarp formation. The fact that there is also 231 m of extra material on top of the model surface where it is at its highest point means that it is likely that this much extra material has also been removed in these locations. This analysis suggests that adjacent to these scarps there has been of the order of several hundred meters of material removed. The lack of any significant amount of debris at the base of these scarps implies either erosion of very clean ice or efficient removal of any nonvolatile debris by eolian action. It is worth noting this is net erosion: there may have been several cycles of deposition and erosion that cannot be detected today. However, we argue in section 6 that there has only been one (perhaps ongoing) major erosional episode.

[71] The concentrated removal of material at the scarp locations implies a strong feedback mechanism for scarp growth. The fact that there are only a handful of scarps between the edge of the SPLD and their summit and that each scarp requires the removal of so much material may imply that the timescale for scarp initiation is considerably longer than the timescale for scarp evolution once initiated.

[72] Although a relative chronology of south polar history is starting to appear, assigning absolute dates or timescales to these events and processes is still not possible at this time. We discuss the timing of scarp formation further in section 6.

5. Unpredicted Exposures

[73] As part of this study we also inspected all scarps to the west of the initial study area to look for other outcrops of this same bench-forming layer, BFL_3. We have not extended this search to the east of the initial study area, as the situation there is complicated by the influence of the buried portion of the Prometheus impact basin. We defer analysis of that region to future work. There are many resistant benches visible in the western region. We mapped only those which were a convincing match with the bench-forming layer (BFL_3 in Figure 4) on the basis of its morphology and that of the surrounding strata. The distribution of these morphological matches is shown in the top panel of Figure 15. It includes exposures already discussed in sections 2.2 and 4.

[74] As an example of what we considered a good geomorphologic match we show an image pair comparing exposures from the originally mapped eastern scarp and the scarp furthest from this (bottom panel in Figure 15). This particular exposure, shown in Figure 15b, is interesting because the base of that scarp rests upon southern highland material rather than additional layered deposits. All of the salient geomorphologic features noted in section 2.2 and Figure 4 are repeated on this distant scarp. The main bench-forming layer (BFL_3), the superposed "wavy" layers (WL), the lower sequence of fine layers (SS_3) and the upper sequences of fine layers (SS_1 and SS_2) separated by the same prominent double layer (BFL_2, marked with arrows) are visible on both scarps. These two scarps are separated by ~385 km laterally with scarp A being ~1600 m higher than scarp B. The maximum correlation distance between mapped exposures of BFL_3 over the whole SPLD is ~500 km.

[75] The bench-forming layer we have mapped or modeled (BFL_3) crops out on every major scarp between the center of the SPLD and its periphery in the region to the west of the deposit center. All these scarps at least partially repeat the same stratigraphy. This may mean that the

historical record visible in this region of the SPLD is much smaller than previously expected.

[76] The more distant exposures of BFL_3 (westward of longitude 315°E) shown in the top panel map-view in Figure 15 are mapped on the basis of geomorphology alone. They are not predicted by the approach we have used in section 4, being at much higher elevation than our model surface in those locations. The elevation of the parabolic fit to exposures of BFL_3 near the center of the SPLD declines rapidly. At the periphery of the SPLD the elevation of this function is far below the surface of the bedrock which underlies the SPLD; see, for example, the cross section AA′ in Figure 8. The higher than modeled elevations of these peripheral exposures (e.g., (B) in Figure 15) cannot therefore be explained by any basal topographic influence or post-depositional modification of BFL_3's elevation.

[77] This elevation difference from the model surface is consistent across all the mapped peripheral exposures, i.e., those not predicted in section 4. The magnitude of this elevation difference is greater for those exposures which are furthest from the center of the deposit. Although the parabolic description is extremely accurate in the central region of the SPLD we must modify its behavior at larger distances.

[78] Two possible end-member scenarios for the shape of this stratum are shown by the shaded shapes in Figure 16. Figures 16a and 16b show layer shapes which can both be approximated by parabolas (shown as heavy dashed lines) in the central region of the SPLD. These two scenarios are therefore both consistent with our observations of parabolic behavior in this central region but they show differing deviations from this behavior at the SPLD margins.

[79] Exposures at the SPLD margin of layers following the shape shown in Figure 16a would be at lower elevation than a parabolic fit to the central region would predict. Conversely, exposures at the SPLD margin of layers following the shape shown in Figure 16b would be at higher elevation than a parabolic fit to the central region would predict. If these mapped bench-forming layers do indeed correspond to the same stratigraphic surface (BFL_3) that we have been investigating then we can distinguish between the two possibilities described above. The higher than predicted elevation of BFL_3 on scarps at the periphery of the SPLD points to Figure 16b as being the most correct approximation of the shape of BFL_3 inside this region of the SPLD.

[80] The shape of the stratum shown in Figure 16b is suitable for the region of the SPLD which is west of the original study area, i.e., longitudes 0°E–90°E. The shape of BFL_3 in the region east of the original study area is governed by the previously described parabolic shape and influenced by the basal topography of the Prometheus impact basin. We will investigate the shape of BFL_3 at the

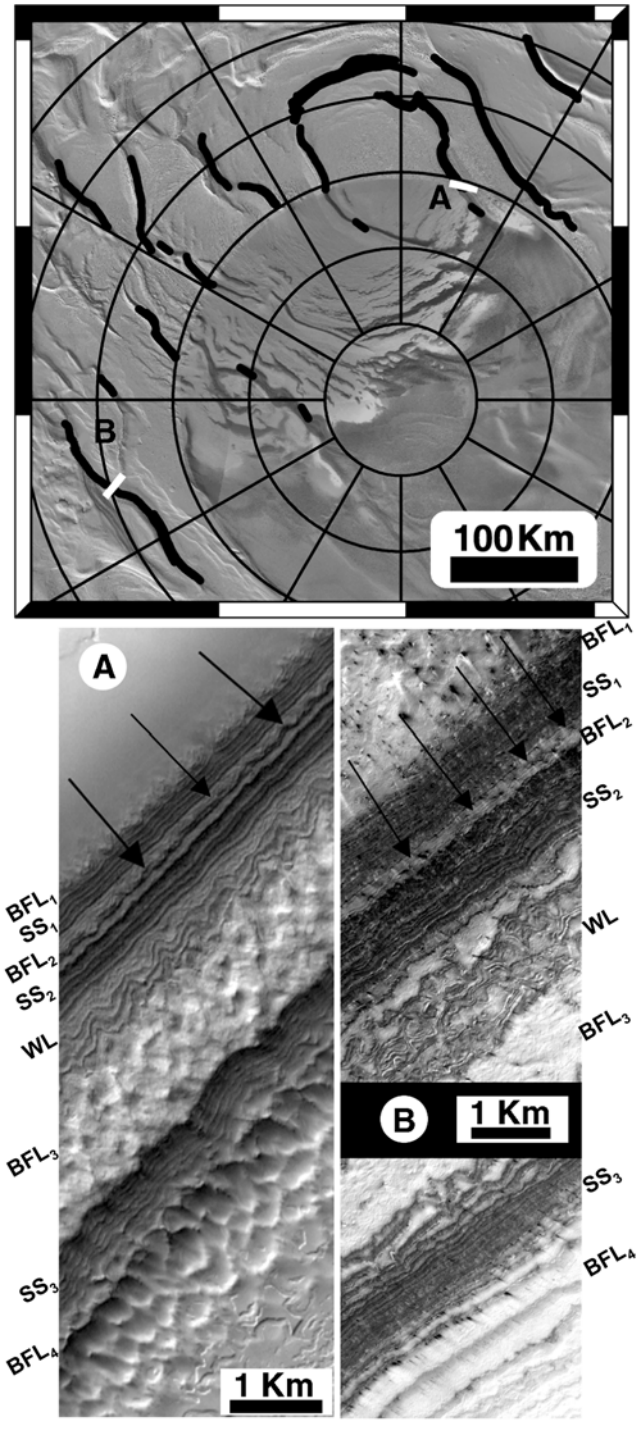

Figure 15. Top panel shows MOLA shaded relief and Viking MDIM (poleward of 87°S) with exposures where BFL_3 has been mapped shown as heavy black lines. Parallels and meridians plotted every 1° and 30°, respectively. Exposures of BFL_3 west of 315°E have been mapped on the basis of similar geomorphology to the type section on the eastern scarp of the original study area (see Figure 4). As an example of what we considered a good geomorphologic match, the two bottom panels compare layering at a distant location (B, indicated in top panel) to the original type section on the eastern scarp (A). These images are separated by over 350 km, with A being 1600 m higher in elevation than B. Annotations have the same meaning as in section 2.2 and Figure 4. The characteristic prominent double layer, BFL_2, is visible in both locations and indicated by arrows. MOC narrow angles are M03/06304 (A, L_s 181°) and M07/05242 (B, L_s 214°), both illuminated from the top left with elevations decreasing from top to bottom. See enhanced version of this figure in the HTML.

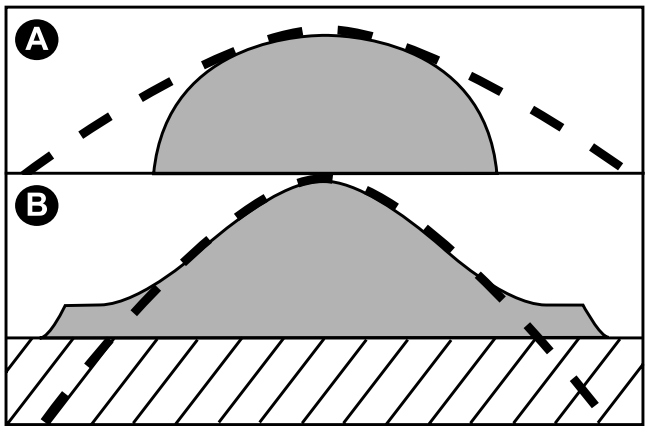

Figure 16. Two possible end-member scenarios for the shape of BFL_3 within the SPLD are shown by the gray areas. Both of these cases can be well approximated by parabolic surfaces in their central regions (heavy dashed lines). Figure 16a shows a shape where elevations decrease more rapidly than a centrally fit parabola would indicate. Figure 16b shows a shape where elevations decrease less rapidly than a centrally fit parabola would indicate. On the basis of our observations, the layering shown in Figure 16b most closely approximates the situation within the south polar layered deposits.

periphery of the SPLD in this eastern region in future studies.

6. Discussion

[81] The results detailed in previous sections have many implications which, below, are explored and discussed in relation to both the erosional history of the SPLD and flow processes that may have acted on these deposits.

6.1. Implications for Erosional History

[82] In section 4.2 we showed evidence that the basal topography associated with the edge of the Prometheus impact basin was influencing the shape of the internal strata. In retrospect it is not surprising that the strata would be offset from their expected locations in this region. As previously mentioned the relief of the basin ($\sim$0.8–0.9 Km) is significant compared to the SPLD thickness in this area ($\sim$3 Km). Any layers deposited on this topography would drape over the edge of the impact basin, and so strata in this area would acquire a different shape than they would elsewhere.

[83] It is interesting that there does not appear to be any surface topography associated with this buried feature. Yet the shape of BFL_3 has been influenced and it is only a few hundred meters below the surface. One interpretation is that a surface topographic signature of the Prometheus basin existed when BFL_3 was deposited. More material than currently exists was subsequently deposited and afterward removed by an episode of erosion. This erosional episode may be associated with scarp migration in this area. This erosion and the possible redeposition of eroded material on the flat interscarp regions (see Figure 9) may have erased the surface signature of basal topography. If that is the case, there may have been no erosional episodes of that magnitude before BFL_3 was deposited, because the topographic signature of the Prometheus basin still existed at that point.

[84] The surface of the present day SPLD is not perfectly parabolic, being incised by many scarps. If a fresh layer were deposited today it would follow this imperfect shape and not be well approximated by a parabolic function at the scale we have been examining these exposures. This would seem to imply that when BFL_3 was deposited there were no scarps or other major surface features on the SPLD (except for the signature of the Prometheus basin basal topography described above). The present scarps may then be something of an anomaly and not representative of the typical appearance of the SPLD through out its history. This is consistent with evidence outlined in the previous paragraph, for a lack of major erosional episodes before the deposition of BFL_3.

[85] The analysis of crater size distribution on the SPLD lends some additional support to the occurrence of this major erosional episode. *Koutnik et al.* [2002] report a much smaller population of small craters (<1 Km) relative to that expected from the observed number of larger (>1 Km) craters. They suggest an episode of SPLD surface modification that may have degraded large craters and completely erased smaller ones. On the basis of the accumulation of small craters since that time, they date this modification episode to have occurred $\sim 10^5$ years ago. This is extremely recent compared to the surface age they retrieve from the larger craters of $3-10 \times 10^7$ years. Uncertainties inherent in using craters to date a surface may mean that these timescales are not correct in an absolute sense, but the large difference between them should be a robust result. Their proposed modification episode may coincide with the erosional episode proposed above.

[86] The above arguments would seem to imply that the scarps may be considerably younger than the deposits which they incise.

[87] An interesting characteristic of the model surface is that BFL_3 is predicted to crop out close to the current rim of the M^{c}Murdo impact crater (see Figure 8). It is plausible that this is the case; however, the highly disrupted nature of the terrain in this area and the removal of overlying strata make it impossible at present to confirm. On the basis of the cross section BB′ shown in Figure 8 the region to the north of the initial study area appears to have had material removed over a large area. The observed presence of the M^{c}Murdo secondary impact craters may indicate that any removal of this material occurred prior to that impact. It is possible that the impact occurred before this removal episode if the secondary crater field is being exhumed; however, it seems unreasonable to assume that the all parts of the crater field would be exhumed simultaneously. The implication is that the M^{c}Murdo impact postdates the erosional episode described above.

[88] As mentioned in section 4.5 a relative chronology of events which have modified the SPLD is emerging. On the basis of the investigations presented in this paper we propose the following sequence of events.

[89] 1. The upper few hundred meters of the layered deposits, including BFL_3 and surrounding sequences, are emplaced. They were draped over a pre-existing

dome-shaped object with a shape similar to that shown in Figure 16b.

[90] 2. The SPLD enter into a period of retreat. Scarps are formed at the periphery and interior of the layered deposits. The curvature of the internal layers indicates the overall extent of the layered deposits was not much reduced (see Figure 2). The region north of the study area may have had material removed without forming large scarps. Some of the material eroded from retreating scarps may be redeposited on flat interscarp areas (see Figure 9). The SPLD surface topography associated with the buried portion of the Prometheus impact basin is removed.

[91] 3. The crater M^{c}Murdo forms and creates a field of secondary impact craters. Since these secondaries are still visible, the impact must have occurred after most of the erosion described above.

[92] 4. Ongoing reworking of SPLD material has possibly degraded these secondary craters and resulted in further scarp retreat. The M^{c}Murdo crater may have been enlarged by preferential sublimation since its walls can retreat in the same way as scarps.

[93] Assigning absolute ages to these events is difficult. The extremely small area of the surface of BFL_3 currently visible means no reliable estimate of how long it was exposed to impacts can be made. We have identified only one impact crater ($\sim$2.8 Km) on BFL_3 which is currently being exhumed by retreat of the overlying strata (at 85.312°S, 311.233°E, see MOC image M03/04191). BFL_3 is constrained to be older than the current surface of the layered deposits, estimates of which range from 10 to 100 Myr [*Plaut et al.*, 1988; *Herkenhoff and Plaut*, 2000; *Koutnik et al.*, 2002]. In our interpretation, there may be a considerable period of time between stages 1 and 2 above, during which no major modification of the SPLD took place.

[94] In the sequence of events proposed above, the surface age of the layered deposits, measured from crater abundances, reflects the length of time between the deposition of the upper section and the present. This age estimate is complicated by the fact that the area of this older surface is continuously shrinking as scarps retreat and material is possibly reworked into flat lying layers on the interscarp regions. The surface age may therefore vary from location to location within the SPLD. The differing surface ages inferred from different crater size ranges [*Koutnik et al.*, 2002] attests to size-dependent modification of the crater population, which also complicates estimation of surface age.

[95] Ablation of flat surfaces is expected to be less efficient than erosion by migrating scarps. A protective sublimation lag, which retards further sublimation, can quickly develop on a flat dusty ice surface [*Hofstadter and Murray*, 1990]. Such protection can be more easily removed from a sloping surface by mass wasting and enhanced wind erosion. In addition, equatorward slopes receive greater amounts of solar energy. The broad flat plateau of SPLD which extends equatorward in the longitude range 150°E–240°E has fewer scarps. It may record a crater population that dates from the end of the depositional period. Considering the cratering record of this region alone may better constrain the age of the depositional period. This in turn will place an upper bound on the length of time over which all the subsequent events, outlined above, occurred.

6.2. Implications for Flow Processes

[96] The extent to which the northern or southern polar layered deposits experience flow is currently a major open question [*Clifford et al.*, 2000]. Constraints on the importance of flow processes come from two lines of evidence, firstly the undistorted nature of these layers near scarps and secondly the overall shape of the BFL_3 stratum.

[97] *Hvidberg* [2003] and *Fisher* [2000] have investigated layer shapes expected within a flowing ice cap undergoing accumulation with scarps undergoing ablation. They find that considerable waviness and discontinuities are to be expected in such a situation. However, if there is no flow, then layers would not have these characteristics. We find that a simple polynomial can predict layer elevations over hundreds of kilometers, indicating that the large-scale waviness of internal strata predicted by *Hvidberg* [2003] and *Fisher* [2000] is not present in the SPLD. This is consistent with a situation where flow has not occurred at significant rates since the scarps began forming.

[98] To investigate whether flow could have played a significant role before the scarps were formed, we consider the shape of the SPLD when BFL_3 was deposited. BFL_3 represents a paleosurface of the SPLD. We argued in the preceding paragraph that this shape has not been distorted by flow processes. The current shape of BFL_3 is therefore representative of the shape of the SPLD on which it was deposited.

[99] Interpreting the surface shape of an ice cap as a diagnostic of flow processes is possible only if the surface mass-balance distribution (and its history) is known. *Ivanov and Muhleman* [2000] have analyzed the shape of the north polar layered deposits and found that mass-balance processes can reproduce its observed shape without material flow. [*Greve et al.*, 2004] have modeled the formation of the north polar layered deposits including both mass-balance and flow processes and concluded that flow has had a small effect on their overall shape. No direct measurements of the current surface mass balance over the SPLD have been made; however, it is unlikely that these current rates reflect the long term average. The age of BFL_3 is constrained to be older than the surface age of the SPLD, estimates of which range from 10 to 100 Myr [*Plaut et al.*, 1988; *Herkenhoff and Plaut*, 2000; *Koutnik et al.*, 2002]. This indicates that BFL_3 has been in place for many obliquity cycles, during which the surface mass balance may have changed significantly.

[100] The long-term mass balance of the SPLD before the deposition of BFL_3 is unknown. As noted in the previous section, the continuous nature of BFL_3 indicates that the polar deposits which it covers did not have major scarps. The narrow ablation zones (troughs and scarps) which characterize the present polar deposits may not have been present. The results discussed in the previous subsection also imply that there were no major erosional episodes until after BFL_3 was deposited. Formation of sublimation lag deposits make it unlikely that flat areas on these polar deposits could remain in a negative mass balance regime for long.

[101] BFL_3 was deposited over a large area, which suggests that the mass-balance distribution at that time might have been fairly uniform. Without further information, a reasonable first assumption for the mass-balance distribution of the SPLD before the deposition of BFL_3 is that of accumulation at some spatially uniform rate (which may be zero). In reality the mass-balance distribution is likely to be complicated by spatial variations in the availability of water vapor as well as the nature of the surface on which deposition occurs. It is possible that there may have been residual CO_2 ice covering some areas of the SPLD during this epoch, which would lead to enhanced deposition over those locations. However, the assumption of accumulation at some spatially uniform rate (which may be zero) is not an unreasonable starting position.

[102] The steady-state shape of an ice cap undergoing flow and uniform accumulation is described by a Vialov profile [*Vialov*, 1958; *Paterson*, 1994]. This profile is similar in shape to the shaded volume shown in Figure 16a. Elevation decreases and surface slope increases toward the margin, where the elevation goes to zero and the surface slope to infinity (except in detailed theories which accurately describe the local slope near the margins). The case of zero accumulation and ablation [*Halfar*, 1981] gives a profile with similar properties to a Vialov profile (see Figure 1 of *Nye* [2000]), although the aspect ratio of the Halfar profile decreases with time. This model has been adapted by *Nye* [2000] to study flow in both northern and southern layered deposits. These models assume no basal sliding with all motion being attributed to shear within the ice.

[103] We can consider the region west of the original study area (longitudes 0°E–90°E) where we feel the internal shape of BFL_3 is best described. The shaded area in Figure 16b shows the shape of that stratum in this region and so describes the shape of the SPLD over which it was deposited.

[104] The distinction between the two end-member scenarios illustrated in Figure 16 (see section 5) is important, as it addresses the question of the significance of any flow processes that have acted on the SPLD. Figure 16a shows an SPLD shape which is similar to the Vialov and Halfar profiles discussed above. This shape would be consistent with flow having a dominant role in the overall shaping of the SPLD. However, as discussed in section 5, the elevations of exposures of BFL_3 at the periphery of the SPLD indicate that this internal layer (and so the shape of the SPLD when it was deposited) is instead approximated by Figure 16b.

[105] Here we consider possible reasons why the SPLD are not shaped in the same way as these theoretical profiles. Crucially, the assumption of a steady-state form may not be valid if ice flow within the SPLD has been too sluggish to respond quickly to changes in surface mass balance. However, if we do assume a near steady-state ice cap then the shape shown in Figure 16b has interesting implications. First, mass balance could have been distributed nonuniformly, with ablation vanishing near the margins so that the cap profile can be concave there; this is atypical of terrestrial ice sheets. Alternatively, if one assumes uniform mass balance, then the observed shape would imply an unusual distribution of radial flow velocity. One method of accounting for this is to consider spatial variations in ice viscosity, notably, in the rate coefficient of the ice-flow law (e.g., Glen's Law [*Paterson*, 1994]). In this case the resulting implications on ice composition and temperature within the SPLD would warrant further investigation.

[106] Further understanding of the historical mass balance and SPLD flow properties are needed to uniquely relate the shape of these isochrones to flow history.

7. Summary

[107] We now have a first-order picture of the internal structure of the SPLD. Significant additional complexity not revealed in this analysis is likely to exist. However, this first-order picture answers some of the questions posed in section 1 and also helps in beginning to organize a relative chronology of events that have modified these deposits. We can now return to the questions originally posed in section 1.

[108] 1. Was the deposition regional in scale or local? The deposition of the upper section of the SPLD was regional in scale with layering both correlating over long distances on individual scarps and repeating from scarp to scarp. Confirmed occurrences of the set of strata surrounding BFL_3 now span hundreds of kilometers. The mechanics of the depositional process appear to be robust and not sensitive to local perturbations.

[109] 2. Are the current SPLD a remnant of a formerly larger deposit or is their current extent representative of their historical size? Strata in the central portion of the SPLD are well approximated by a parabolic dome. The fact that these strata are curved to this extent and not flat indicates that when they were deposited they were draped over a dome shaped object similar in size or smaller than the current SPLD, i.e., consistent with Figure 2, A–A′. This rules out a scenario where the SPLD were much larger and then eroded back into a remnant form as depicted in Figure 2, B–B′.

[110] 3. How much does the basement topography affect the shape of the interior strata? We have seen that the basement topography can play a role in the shape of the interior strata even when there is no effect on the current topography. We can observe the offsetting of the internal strata from their expected position in the region near the edge of the Prometheus impact basin. This is likely to represent the most extreme basal topography variations underneath the south polar layered deposits, as we estimate the relief of this basin to be a substantial fraction of the SPLD thickness.

[111] 4. Has the interior of the SPLD been deformed by local/regional processes such as faulting/flow? The interior of the SPLD does not seem to be disturbed by large-scale faulting. The elevations of BFL_3 farther from the center of the deposit indicate that the strata are shaped in a manner consistent with that shown in Figure 16b which is dissimilar from forms that are dominated by flow. The undistorted nature of the layering near scarps means that flow processes are too sluggish to have contributed to their modification. Flow of the ice always occurs at some rate; the pertinent question is whether this rate has any significance over geologic timescales. We have been able to assess that this rate is slow relative to other processes such as ablation. Further analysis of the SPLD interior should enable more progress to be made on this question.

[112] We have shown that the shape of the internal strata is such that the upper few hundred meters of layered deposit material is exposed on many of the scarps between the summit and the base of the SPLD. Since different scarps contain redundant stratigraphic information, there may be a shorter historical record represented in exposures of the SPLD than previously thought.

[113] BFL_3 (and other bench-forming layers like it) has mechanical properties that are distinct from most of the layers in these deposits. Its higher resistance to erosion may be due to a higher sediment content which limits its sublimation rate. This may imply that this layer represents a disconformity within the deposits. It may have been present on the surface for a longer than typical amount of time and so was devolatilized to a greater extent than other strata. As discussed in section 6 the single impact crater we have identified on this stratum does not allow us to estimate how long it was exposed at the surface. Alternatively a higher sediment to ice ratio could be explained by increased dust fallout (perhaps due to intense dust storm activity), lower availability of atmospheric water or even deposition of volcanic or impact debris during its formation.

[114] This study applies only to the upper few hundred meters of the stratigraphic column. Stratigraphically lower layers may show different behavior. There may also be buried remnants of polar deposits from previous epochs (such as the Hesperian ice sheet discussed by *Head and Pratt* [2001]) which form the core of the current SPLD. The existence of such a paleo-polar deposit as the core of the SPLD may be the reason for its 3° offset from the current rotational pole. Such questions could possibly be answered by surface-penetrating radar from orbit but may have to wait for in situ seismic, radar or drilling probes.

[115] This technique of using mathematical fits to enhance stratigraphic studies shows promise for the future. Exposures in disparate locations can be confirmed to belong to the same stratigraphic surface. Additionally dip information, which is difficult to infer from surface mapping alone, can be extracted from this three-dimensional approach. This paper has taken the first steps in developing a conceptual picture of the interior of the SPLD. Bench-forming layers such as BFL_3 provide useful marker beds for further stratigraphic studies, as they form a natural system for dividing up the stratigraphy in the SPLD.

[116] The possibility of independently confirming the internal structure of the SPLD and uncovering the basal topography exists through the use of surface-penetrating radar from orbit. The MARSIS instrument aboard the Mars Express spacecraft and the SHARAD instrument aboard the 2005 Mars Reconnaissance Orbiter are two such possibilities. Identification of an individual stratum such as the bench-forming layer discussed in this paper depends on whether it has a high enough dielectric contrast with the surrounding layers. It certainly has distinct mechanical properties and the hope for these future observations is that these two characteristics will be correlated. However, the chances of successfully retrieving the basement topography are higher, and we eagerly anticipate this new information.

[117] **Acknowledgments.** This work is only possible because of the superb polar DEMs produced by Greg Neumann of the MOLA team. We benefited greatly from discussing these results with Felix Ng, Mimi Gerstell, Bruce Murray, and Andy Ingersoll. We thank Eric Kolb and Ken Tanaka for providing the geologic outlines used in Figure 1. This manuscript was greatly improved by the review comments of Ken Herkenhoff and an anonymous reviewer. S.B. gratefully acknowledges the funding provided by Bruce Murray and Maria Zuber while completing this work. A.B.I. acknowledges funding from the Mars Odyssey participating scientist program.

References

Budd, W. F., D. Jenssen, J. H. I. Leach, I. N. Smith, and U. Radok (1986), The north polar cap of Mars as a steady-state system, *Polarforschung*, *56*, 43–63.

Byrne, S., and A. P. Ingersoll (2003), A sublimation model for Martian south polar ice features, *Science*, *299*, 1051–1053.

Byrne, S., and B. C. Murray (2002), North polar stratigraphy and the paleo-erg of Mars, *J. Geophys. Res.*, *107*(E6), 5044, doi:10.1029/2001JE001615.

Christensen, P. R., et al. (2003), Morphology and composition of the surface of Mars: Mars Odyssey THEMIS results, *Science*, *300*, 2056–2061.

Clifford, S. M., et al. (2000), The state and future of Mars polar science and exploration, *Icarus*, *144*, 210–242.

Cutts, J. (1973a), Wind erosion in Martian polar regions, *J. Geophys. Res.*, *78*(20), 4211–4221.

Cutts, J. (1973b), Nature and origin of layered deposits of Martian polar regions, *J. Geophys. Res.*, *78*(20), 4231–4249.

Cutts, J. A., and B. H. Lewis (1982), Models of climate cycles recorded in Martian polar layered deposits, *Icarus*, *50*, 216–244.

Fishbaugh, K. E., and J. W. Head (2001), Comparison of the north and south polar caps of Mars: New observations from MOLA data and discussion of some outstanding questions, *Icarus*, *154*, 145–161.

Fisher, D. A. (1993), If Martian ice caps flow—Ablation mechanisms and appearance, *Icarus*, *105*, 501–511.

Fisher, D. A. (2000), Internal Layers in an "accublation" ice cap: A test for flow, *Icarus*, *144*, 289–294.

Fisher, D. A., D. P. Winebrenner, and H. Stern (2002), Lineations on the "white" accumulation areas of the residual northern ice cap of Mars: Their relation to the "accublation" and ice flow hypothesis, *Icarus*, *159*, 39–52.

Greve, R. (2000), Waxing and waning of the perennial north polar H_2O ice cap of Mars over obliquity cycles, *Icarus*, *144*, 419–431.

Greve, R., V. Klemann, and D. Wolf (2003), Ice flow and isostasy of the north polar cap of Mars, *Planet. Space Sci.*, *51*, 193–204.

Greve, R., R. A. Mahajan, J. Segschneider, and B. Grieger (2004), Evolution of the north-polar cap of Mars: A modelling study, *Planet. Space Sci.*, *52*, 775–787.

Halfar, P. (1981), On the dynamics of the ice sheets, *J. Geophys. Res.*, *86*, 11,065–11,072.

Head, J. W. (2001), Mars: Evidence for geologically recent advance of the south polar cap, *J. Geophys. Res.*, *106*(E5), 10,075–10,087.

Head, J. W., and S. Pratt (2001), Extensive Hesperian-aged south polar ice sheet on Mars: Evidence for massive melting and retreat, and lateral flow and ponding of meltwater, *J. Geophys. Res.*, *106*(E6), 12,275–12,300.

Herkenhoff, K. E. (2001), Geologic map of the MTM-85,000 Quadrangle, Planum Australe region of Mars, *U.S. Geol. Surv. Misc. Invest. Ser.*, *Map I-2686*.

Herkenhoff, K. E., and B. C. Murray (1990a), Color and albedo of the south polar layered deposits on Mars, *J. Geophys. Res.*, *95*(B2), 1343–1358.

Herkenhoff, K. E., and B. C. Murray (1990b), High-resolution topography and albedo of the south polar layered deposits on Mars, *J. Geophys. Res.*, *95*(B7), 14,511–14,529.

Herkenhoff, K. E., and J. J. Plaut (2000), Surface ages and resurfacing rates of the polar layered deposits on Mars, *Icarus*, *144*, 243–253.

Herkenhoff, K. E., and A. R. Vasavada (1999), Dark material in the polar layered deposits and dunes on Mars, *J. Geophys. Res.*, *104*(E7), 16,487–16,500.

Herkenhoff, K. E., L. A. Soderblom, and R. L. Kirk (2003), Stratigraphy and structure of the south polar layered deposits on Mars, paper presented at Third International Conference on Mars Polar Science and Exploration, Lunar and Planet. Inst., Lake Louise, Alberta, Canada.

Hofstadter, M. D., and B. C. Murray (1990), Ice sublimation and rheology—Implications for the Martian polar layered deposits, *Icarus*, *84*, 352–361.

Howard, A. D. (1978), Origin of the stepped topography of the Martian poles, *Icarus*, *34*, 581–599.

Howard, A. D. (2000), The role of eolian processes in forming surface features of the Martian polar layered deposits, *Icarus*, *144*, 267–288.

Hvidberg, C. S. (2003), Relationship between topography and flow in the north polar cap of Mars, *Ann. Glaciol.*, *37*, 363–369.

Ivanov, A. B., and D. O. Muhleman (2000), The role of sublimation for the formation of the northern ice cap: Results from the Mars Orbiter Laser Altimeter, *Icarus*, *144*, 436–448.

Kieffer, H. H. (1979), Mars south polar spring and summer temperatures: A residual CO_2 frost, *J. Geophys. Res.*, *84*, 8263–8288.

Kolb, E. J., and K. L. Tanaka (2001), Geologic history of the polar regions of Mars based on Mars Global Surveyor data, II. Amazonian period, *Icarus*, *154*, 22–39.

Koutnik, M., S. Byrne, and B. Murray (2002), South polar layered deposits of Mars: The cratering record, *J. Geophys. Res.*, *107*(E11), 5100, doi:10.1029/2001JE001805.

Malin, M. C., and K. S. Edgett (2001), Mars Global Surveyor Mars Orbiter Camera: Interplanetary cruise through primary mission, *J. Geophys. Res.*, *106*(E10), 23,429–23,570.

Mellon, M. T. (1996), Limits on the CO_2 content of the Martian polar deposits, *Icarus*, *124*(1), 268–279.

Murray, B. C., L. A. Soderblom, J. A. Cutts, R. P. Sharp, D. J. Milton, and R. B. Leighton (1972), Geological framework of the south polar region of Mars, *Icarus*, *17*, 328–345.

Murray, B., M. Koutnik, S. Byrne, L. Soderblom, K. Herkenhoff, and K. L. Tanaka (2001), Preliminary geological assessment of the northern edge of Ultimi Lobe, Mars south polar layered deposits, *Icarus*, *154*, 80–97.

Neumann, G. A., D. D. Rowlands, F. G. Lemoine, D. E. Smith, and M. T. Zuber (2001), Crossover analysis of Mars Orbiter Laser Altimeter data, *J. Geophys. Res.*, *106*(E10), 23,753–23,768.

Ng, F., and H. Conway (2004), Fast-flow signature in the stagnated Kamb Ice Stream, West Antarctica, *Geology*, *32*(6), 481–484.

Ng, F. S. L., and M. T. Zuber (2003), Albedo feedback in the patterning mechanisms of Martian polar caps, paper presented at Third International Conference on Mars Polar Science and Exploration, Lunar and Planet. Inst., Lake Louise, Alberta, Canada.

Nye, J. (2000), A flow model for the polar caps of Mars, *J. Glaciol.*, *46*(154), 438–444.

Nye, J. F., W. B. Durham, P. M. Schenk, and J. M. Moore (2000), The instability of a south polar cap on Mars composed of carbon dioxide, *Icarus*, *144*, 449–455.

Paige, D. A., and K. D. Keegan (1994), Thermal and albedo mapping of the polar regions of Mars using Viking thermal mapper observations: 2. South polar region, *J. Geophys. Res.*, *99*(E12), 25,993–26,013.

Paterson, W. S. B. (1994), *The Physics of Glaciers*, 3rd ed., Pergamon, New York.

Pelletier, J. D. (2004), How do spiral troughs form on Mars?, *Geology*, *32*(4), 365–367.

Plaut, J. J., R. Kahn, E. A. Guinness, and R. E. Arvidson (1988), Accumulation of sedimentary debris in the south polar region of Mars and implications for climate history, *Icarus*, *76*, 357–377.

Prettyman, T. H., et al. (2004), Composition and structure of the Martian surface at high southern latitudes from neutron spectroscopy, *J. Geophys. Res.*, *109*, E05001, doi:10.1029/2003JE002139.

Seidelmann, P. K., et al. (2002), Report of the IAU/IAG Working Group on Cartographic Coordinates and Rotational Elements of the Planets and Satellites: 2000, *Celest. Mech. Dyn. Astron.*, *82*, 83–111.

Sharp, R. P., B. C. Murray, R. B. Leighton, L. A. Soderblom, and J. A. Cutts (1972), The surface of Mars: 4. South polar cap, *J. Geophys. Res.*, *76*, 357–368.

Smith, D. E., et al. (2001), Mars Orbiter Laser Altimeter: Experiment summary after the first year of global mapping of Mars, *J. Geophys. Res.*, *106*(E10), 23,689–23,722.

Snyder, J. P. (1987), *Map projections—A working manual*, *U.S. Geol. Surv. Prof. Pap.*, *1395*, 383 pp.

Tanaka, K. L., and D. Scott (1987), Geologic map of the polar regions of Mars, *U.S. Geol. Surv. Misc. Invest. Ser.*, *Map I-1802-C*.

Thomas, P. C., S. W. Squyres, K. E. Herkenhoff, A. Howard, and B. C. Murray (1992), Polar deposits of Mars, in *Mars*, edited by H. H. Kieffer et al., pp. 767–795, Univ. of Ariz. Press, Tucson.

Titus, T. N., H. H. Kieffer, and P. R. Christensen (2003), Exposed water ice discovered near the south pole of Mars, *Science*, *299*, 1048–1051.

Tokar, R. L., R. C. Elphic, W. C. Feldman, H. O. Funsten, K. R. Moore, T. H. Prettyman, and R. C. Wiens (2003), Mars Odyssey neutron sensing of the south residual polar cap, *Geophys. Res. Lett.*, *30*(13), 1677, doi:10.1029/2003GL017316.

Vasavada, A. R., J. Williams, D. A. Paige, K. E. Herkenhoff, N. T. Bridges, R. Greeley, B. C. Murray, D. S. Bass, and K. S. McBride (2000), Surface properties of Mars' polar layered deposits and polar landing sites, *J. Geophys. Res.*, *105*(E3), 6961–6970.

Vialov, S. S. (1958), Regularities of glacial shields movement and the theory of plastic viscous flow, in *Symposium at Chamonix 1958—Physics of the Movement of Ice*, *Int. Assoc. Sci. Hydrol. Publ.*, *47*, 266–275.

Ward, W. R. (1973), Large-scale variations in obliquity of Mars, *Science*, *181*, 260–262.

Weijermars, R. (1986), The polar spirals of Mars may be due to glacier surges deflected by Coriolis forces, *Earth Planet. Sci. Lett.*, *76*, 227–240.

Wilhelms, D. E. (1973), Comparison of Martian and lunar multiringed circular basins, *J. Geophys. Res.*, *78*, 4084–4095.

S. Byrne, Department of Earth and Planetary Sciences, Massachusetts Institute of Technology, 77 Massachusetts Avenue, Room 54-510, Cambridge, MA 02139, USA. (shane@quake.mit.edu)

A. B. Ivanov, Jet Propulsion Laboratory, 4800 Oak Grove Drive, Mail-Stop 168-416, Pasadena, CA 91109, USA. (abi@mipl.jpl.nasa.gov)